UNIVERSITY OF TURKU

Hydrothermal synthesis of reduced graphene oxide-cellulose composites for supercapacitor application

Master's Thesis in Materials Chemistry
Department of Chemistry

Author:
Salla-Sofia Mäkinen

Supervisors:
Dr. Lokesh Kesavan
Prof. Carita Kvarnström

13.05.2025
Turku

Master's thesis

Subject: Materials Chemistry
Author: Salla-Sofia Mäkinen
Title: Hydrothermal synthesis of reduced graphene oxide-cellulose composite for supercapacitor application
Supervisors: Dr. Lokesh Kesavan, Prof. Carita Kvarnström
Number of pages: 48 pages
Date: 13.05.2025

Abstract

In the modern world, there is an ever-rising demand for new, environmentally friendly and cost-effective solutions for energy storage. Carbon based materials like reduced graphene oxide (rGO) shows promising features for supercapacitor application due toits high surface area, electrical conductivity and chemical stability. To reduce the precursor graphene oxide, without toxic chemicals, a hydrothermal method was used in an inert atmosphere at low temperatures. Our efforts have resulted in a specific capacitance of 199 F/g at 0.25 A/g in 1 M H_2SO_4 for hydrothermally reduced rGO. To compare the performance of the hydrothermal method, chemical and microwave reduction methods were also used and studied using UV-Vis spectroscopy, and electrochemical measurements. A green and sustainable composite combining the conductivity of rGO and mechanical strength of cellulose nanofibers was prepared by a simple sonication-assisted combination process, resulting in a specific capacitance of 167 F/g at 0.25 A/g in 1 M H_2SO_4. Self-standing flexible composite films were prepared using vacuum filtration and characterized using XRD and 4-probe conductivity measurements.

Key words: reduced graphene oxide, hydrothermal reduction, chemical reduction, microwave reduction, nanocellulose, electrochemistry, supercapacitor

Contents

Abbreviations

GO Graphene oxide

rGO Reduced graphene oxide

CNF Cellulose nanofiber

SC Supercapacitor

NMP N-Methyl-2-Pyrrolidone

DMF Dimethylformamide

DMAc Dimethylacetamide

EG Ethylene glycol

EDLC Electric double layer capacitance

CV Cyclic voltammetry

GCD Galvanostatic charge/discharge

EIS Electrical impedance spectroscopy

UV-Vis Ultraviolet-visible

XRD X-ray diffraction

WE Working electrode

RE Reference electrode

CE Counter electrode

1 Introduction

Graphene is a two-dimensional material with a basal plane consisting of a monolayer of sp^2 hybridized carbon atoms in a honeycomb lattice structure. Graphene was theoretically predicted a long time ago, and was first isolated and characterized by Andre Geim and Konstantin Novoselov in 2004.[1] They were later awarded with the Nobel Prize in physics in 2010. Graphene is a very attractive material for many applications for its superior mechanical, electrical and thermal properties compared to traditional inorganic materials. Although graphene has many excellent properties, like extraordinary transparency and great electronic properties, it also has no bandgap and poor water solubility, limiting its applications greatly in some areas. The production of cheap high-quality graphene at an industrial scale also remains a challenge.[2]

Building on graphene's trend, graphite oxide, originally discovered over 150 years ago, regained significant research interest as a precursor for cost-effective mass production of graphene materials[2].Graphite oxide has the layered structure of graphite, but also has oxygen containing functional groups making it hydrophilic. Due to the oxygen functionalities, the conjugated structure is disturbed, making the material's electrical properties fall far below those of graphene. The functional groups also increase the interlayer distance and through exfoliation in water, one of few atoms thick layers can be separated, forming graphene oxide (GO).[3]GO's most interesting property is that it can be reduced to graphene-like sheets as oxygen groups are removed and the conjugated structure is restored. This material is called reduced graphene oxide (rGO).[2]

rGO is considered a middle point between GO and graphene. rGO not only has graphene-like properties like good conductivity, but is also easy to prepare in desired quantities from cheap GO using a variety of different reduction methods.[2] The many different reduction processes and the degree of reduction results in different types of rGO, widening its possible applications. Additionally, rGO still possesses functional groups that can make it dispersible in many solvents. Unfortunately, rGO does struggle with aggregation, which is irreversible and negatively effects its conductive properties which is undesirable for certain applications.[4]

Chemical reduction is a popular method to produce rGO as it is a simple and effective way of producing large amounts of product at a wanted quality. Chemical reduction however often requires using hazardous reducing agents raising environmental concerns, and it can leave

residues on the rGO which can affect its properties.[5] Hydrothermal reduction instead is a promising option for reducing GO as it is environmentally friendly, simple and cost effective. It also has good scalability and can suit large-scale production.[6]

Cellulose is the most abundant natural polymer on earth, known for its non-toxicity, biodegradability and renewability. Cellulose nanofibers (CNFs) are extremely small fibers, with their diameter being in the nanometer scale. The nanoscale dimensions give CNFs a high surface-to-volume ratio, excellent mechanical strengths and enhanced thermal stability. The different uses of CNFs include filtration membranes, biomedical uses and reinforcement in composite materials.[7,8]

Supercapacitors (SCs), also known as ultracapacitors and electrochemical capacitors are energy storage devices that are able to store and release energy very quickly. SCs bridge the gap between traditional capacitors and batteries, and have a higher specific power and longer cycle-lives than most batteries. SCs have generated interest in applications for consumer electronics, hybrid electrical vehicles and industrial power management.[9] SCs can store charge through different mechanisms. Electrical double layer capacitors (EDLCs) store charge by accumulating charge at the interface of the electrode and electrolyte. Pseudocapacitors, also called redox capacitors, instead function through a reversible Faradaic-type charge transfer.[10,11]

rGO-CNF composites can offer a low-cost, versatile, flexible and environmentally friendly option for SC applications.[12]In this combination rGO acts as the conductive material, and CNFs add mechanical strength, prevent rGO's aggregation and can enhance the electrode-electrolyte connections to enhance the composite's electrochemical performance compared to just rGO.[13]

1.1 Graphene oxide

The production of GO starts by first producing graphite oxide. The production process of graphite oxide has gone through multiple phases, but all involve treating graphite with strong oxidants and acids[14]. Graphite oxide was first prepared by Brodie[15] in 1859 by treating graphite powder with nitric acid and potassium nitrate. The production method has then been modified in various ways over the years by Staudenmeier[16] in 1898, then by Hofman[17] in 1937 and later in 1958 by Hummers and Offeman[18]. In 2010 Tour and co-workers[19] reported the "modified Hummers method" with an increased reaction yield and higher oxidation rate without the generation of toxic gases.

The basal plane of graphene materials consists of a sp^2-bonded carbon network in a honeycomb lattice. While the exact structure of graphite oxide is hard to determine, the Lerf-Klinowski model is widely accepted[20,21].They concluded there are two different regions in the structure, consisting of an aromatic region with unoxidized benzene rings, and a region with aliphatic six-membered rings. The basal plane is occupied by 1,2-epoxides and hydroxyl groups, and the edges mostly contain carboxyl and hydroxyl groups. Graphite oxide has a multilayer structure similar to graphite, but the added oxygen functionalities not only increase the interlayer distance but also make graphite oxide highly hydrophilic. This results in easy exfoliation as usually the sheets are held by strong van der Waals forces.[22,23] This can be done either by sonication or stirring to produce a homogeneous colloidal GO suspension in either polar organic solvents or aqueous media.[22]

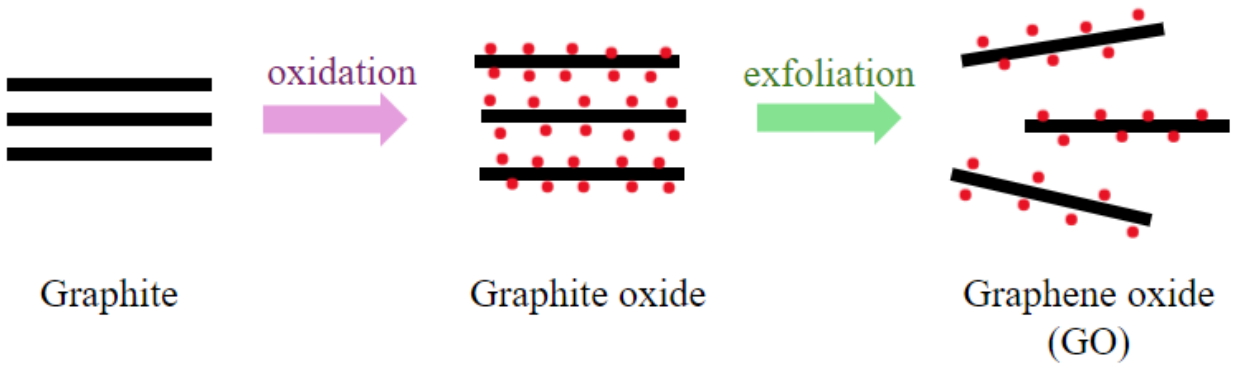

Figure1. Production process from graphite to GO.

GO is chemically similar to graphite oxide but structurally different as it retains the oxygen functionalities, but mainly exists as mono-, bi- or few-layer graphene sheets[14]. Like graphite oxide, GO is also highly hydrophilic[2].

GO is also insulating, as the conductivity of graphene materials primarily depends on the extensive network of connected carbon atoms. Oxidation disrupts the network, causing π-electrons to become localized. This results in a decrease in both the mobility of charge carriers and their overall concentration. The insulating nature of GO is undesirable for some applications, and one of GO's important characteristics is that it can be reduced by removing some of the oxygen containing functional groups and recovering the conjugated structure.[2,22]

GO has applications in various fields. It can address environmental issues such as excess CO_2 and toxic gases like ammonia, acetone and formaldehyde. CO_2 can also be converted through photocatalysis using GO-based composites. GO can also help removing organic dyes and heavy metal ions from water. Additionally, in medicine, GO has promising applications in gene delivery for treating gene delivery, as well as drug delivery for targeting cancer and biosensors. GO membranes also can serve as molecular sieves for gas transport, and in construction, it improves the strength and water resistance of building materials like cement.[24]

1.2 Reduced graphene oxide

rGO is the result when oxygen functionalities are removed from GO. rGO still retains some of the oxygen functionalities, but the restoration of the pi bond conjugation increases the conductivity of rGO making it suitable for energy storage applications.[25] rGO is hydrophobic and has the tendency to agglomerate due to the van der Waals forces, as the repulsion between layers weakens when the functional groups are removed. The agglomeration is irreversible and causes the electrolyte ions to be unable to efficiently infiltrate the material.[26]

The key properties of rGO are its significantly improved in thermal and electrical conductivity from GO. rGO can also have a higher surface area than GO which is important for energy storage applications. Compared to graphene, rGO rarely matches the purity and conductivity of pristine graphene due to the residual oxygen groups and defects. rGO however can benefit from these surface groups, as they enable the possibility for further modifications or functionalization.[27]

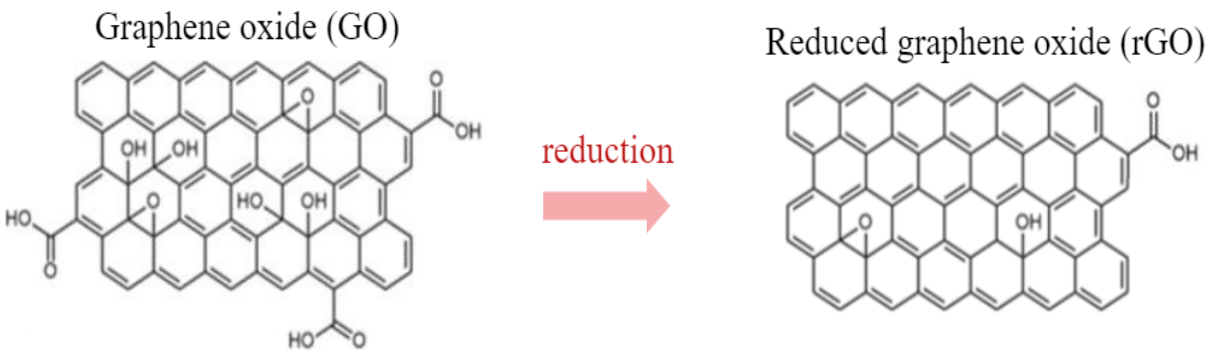

Figure2. Oxygen groups are removed and pi bonds are restored during reduction.

The reduction of GO can be achieved through many different methods, like chemical[5]-, thermal[28]-, electrochemical[29]-, photo[30]-, microwave[31]- and plasma[32] reduction. Different methods can also be combined[33].The reduction process and reaction conditions cause the resulting rGO to have different properties, for example affecting its conductivity. The challenges of reducing GO include controlling the degree of reduction to balance between the retention of functional groups and conductivity, achieving consistent material properties as well as considering the environmental concerns of the reduction process.[34,35]

rGO has versatility when it comes to applications. For energy storage uses like batteries and SCs can benefit from rGO's conductivity and high surface area. rGO can also be used as a conductive material for sensors, transistors and transparent conductive films. The improved conductivity and chemical stability compared to GO can also be utilized for a support material for catalytic reactions. rGO membranes also have possible uses in water purification. Finally, rGO can be used for drug delivery and biosensors.[27,36]

In this study hydrothermal reduction, chemical reduction and microwave reduction methods were used and as such, these three methods will be discussed in more detail.

1.2.1 Hydrothermal reduction

In the hydrothermal reduction process GO undergoes thermal treatment in water under enhanced pressure and temperature in a sealed autoclave. The advantages of the hydrothermal method are the mild reduction conditions, environmental friendliness and simple equipment

requirements, as it can be done with only an autoclave or an oven[37]. Additionally, the hydrothermal method doesn't introduce any non-carbon impurities[38].

Hydrothermal reduction is based on supercritical water. The ionic product of water is high, and the hydrothermal conditions cause -OH groups to protonate, leading to the dehydration on the edges and planes of GO.[39] The closed system with a relatively high temperature and internal pressure also promotes the recovery of π-conjugated system which can minimize defects[40]. Zhou et al. used Raman spectroscopy to demonstrate that the hydrothermal method is more effective in repairing the conjugated carbon network than chemical method like hydrazine induced reduction. They have also concluded that the hydrothermal method is however less effective in reducing the GO compared to other common methods.[38]

This method offers tunability, as initial concentration of the GO dispersion, temperature, reaction time and pH, all affect the properties of the rGO. In a study by Ding et al. they discovered that when using a concentration of 0.3 mg/ml the product dispersed well, but with 0.4 and 0.5 mg/ml the products agglomerated during the reduction.[37]

Higher reaction temperature leads to a more thorough reduction, and in one study they found electrical conductivity to increase as the temperature was increased from 160 – 220°C[41,42].A longer reaction time however doesn't necessarily lead to better electrochemical properties. Ding et al. found that ideal reduction time was over 2h but less than 6h at a temperature higher than 160°C.[37]Another study by Huang et al. concluded that rGO that has been reduced for 2 – 8h have better electronic properties, but continuing the reduction for 10h results in porous and damaged rGO which can instead offer sites for polymerization or metal oxide doping. They also found that GO flakes remain in the reduction up to 4h.[6]

pH has been proven to play an important role in controlling the properties of the resulting rGO. When studying the effects on the morphology and structure of rGO when reduced at a different pH, one study by Ding et al. concluded that acidic pH led to a higher number of defects in the rGO, smaller sheet size and a higher tendency to agglomerate. Basic conditions instead lead to a lower amount of defects.[43]A study by Zhou et al. got similar results, with basic pH leading to a more stable rGO solution, and acidic pH to intense aggregation[38]. In another study conducted by Bai et al. they studied the effects of pH on the electrochemical properties of rGO. They found that neutral and acidic pH lead to the rGO showing both EDLC and pseudocapacitance with a high specific capacitance (230 F/g at 1 A/g), and basic pH lead to mostly EDLC behaviour with lower specific capacitance (185 F/g at 1 A/g).[44]

Solvothermal reduction uses organic or mixed solvents, and compared to the hydrothermal method it can offer more variety in the functionalization and properties in rGO. However, the solvothermal method can result in less pure rGO due to residues form the solvent, and depending on the solvent used can involve toxic or flammable solvents raising both environmental and safety concerns.[39] One setback to both solvothermal and hydrothermal method is the relatively long reaction times required compared to other methods like chemical reduction[39].

1.2.2 Chemical reduction

Chemical reduction uses reductive reagents to remove the oxygen functionalities from GO through redox reactions[33]. Commonly used chemical reducing agents are hydrazine[45,46] and sodium borohydride[47,48], both of which raise concerns for their toxicity[34].A common non-toxic reducing agent is L-ascorbic acid[49,50]. Studies have also been exploring other eco-friendly agents like plant extracts and sugars, but show lower reduction efficiency[35,51,52]. In addition to possible toxicity, another issue of chemical reduction is the possibility of residual byproducts being left on the rGO which require washing to remove. The advantages of chemical reduction are its scalability for large-scale production as well as tunability as different reaction conditions, reducing agents and concentrations lead to different properties of the final rGO.[53]

In this study $NaBH_4$ was used for chemical reduction. The reduction of GO using $NaBH_4$ can be done at relatively mild reaction conditions, with significant increase in conductivity seen at 80°C during the first 10 minutes of the reaction[54]. $NaBH_4$ also shows preference for reducing certain oxygen containing functional groups while not being effective for others[22,54]. The ratio of GO to $NaBH_4$ also affects the reduction process, with a 1:10 ratio showing the highest reduction degree[55].

1.2.3 Microwave reduction

Microwave reduction has been studied as an alternative rapid thermal reduction method, with its main attraction being the short reduction time. Microwave reduction offers easy tunability with reaction time and temperature but does require special equipment.[31,56] The reduction

degree depends on the duration of the microwave treatment at a specific power, with most using at least 800 W when reducing GO in a solvent.[57–61]

Microwave reduction in a solvent has been done in a multitude of different organic solvents, and solvents with amide groups likeN-methyl-2-pyrrolidone (NMP) and dimethylformamide (DMF)have been found to be more effective in reducing GO. It's been reported that it is possible to get similar results to 1h solvothermally reduced GO in 3 – 9 min by using a microwave at 800 W power.[57]

Microwave reduction using water as a solvent seems to lead to a low reduction degree, and is less effective than solvothermal methods[58,59]. In a study by Chen et al.[62] when aqueous GO solution was irradiated using a microwave at 800 W for 1 min, no change in colour occurred. However, in dimethylacetamide (DMAc), it changed to black. They also used a mixture of DMAc and H_2O, and concluded that the presence of water has neither a positive nor a negative effect on the reduction degree.[62]

1.3 Cellulose nanofibers

Cellulose, the most abundant polymer, is renewable, cheap, lightweight and biodegradable, which is why recently cellulose has received a lot of attention for many possible applications in areas like pharmaceuticals, sensors, flexible electronics and flexible displays.[63,64]

CNFs are very fine fibers derived from cellulose. They have a diameter of 5 – 20 nm and can be several micrometres in length. CNFs can be extracted from renewable biomass sources like wood, plants, algae and bacteria. Cellulose is composed of long linear chains of β-D-glucose molecules linked by β-1,4-glycosidic bonds (figure 3). The -OH groups on the chain cause hydrogen bridges to form, resulting in a fibrillated structure. These groups also offer the possibility of chemical modification and compatibility with aqueous systems, giving cellulose a competitive edge for different applications.[36]

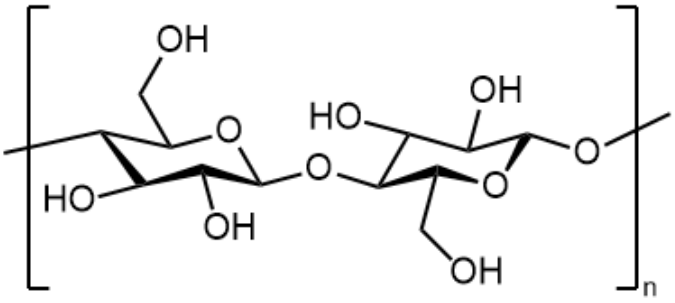

Figure 3. Structure of cellulose.

CNFs have high crystallinity, which contributes to their mechanical properties like high tensile strength and stiffness.[8] CNFs are also highly dispersible in water allowing them to form stable suspensions. CNFs also have moderate thermal stability, depending on the source of the cellulose and treatment, with degradation temperatures ranging from 200 – 300°C[65].

CNFs can be produced by isolating it from different plant materials through several methods including mechanical processes like grinding, microfluidization and high-shear homogenization. Other possible ways are different chemical treatments like acid hydrolysis, TEMPO oxidation, and enzymatic processes.[63]

TEMPO oxidation uses 2,2,6,6-tetramethylpiperidine-1-oxyl, a stable free radical along with other reagents like NaBr and NaClO. After cellulose is derived from wood pulp and any impurities are removed, it is oxidated in an alkaline medium with the fore-mentioned chemicals. The TEMPO radical facilitates the oxidation of primary alcohol groups to carboxyl groups, which enhances the hydrophilicity and dispersibility of the cellulose in water. After oxidation the modified cellulose can then be further processed to produce nanofibers.[66,67]

Some challenges with CNFs are its hydrophilicity, as it can limit its application in water-sensitive environments if not properly modifies. Stability, cost and consistency also raise concerns as commercial scale production is under development and variability in raw material can affect the resulting fibers' dimensions and properties.[68,69]

1.4 Supercapacitors

SCs are advanced energy storage devices that have gained attention due to their unique features and potential applications.SC materials can be divided into different types based on the energy storage method; electrical double layer capacitors (EDLC) and pseudocapacitors. Depending on the material of the electrodes, they can also function simultaneously, which are referred as hybrid capacitors.[11]

Pseudocapacitors store charge through fast and reversible redox reactions at the surface of the active materials. The capacitance of pseudocapacitors can be much higher than EDLCs, but they have lower power density, can suffer from lack of stability during cycling and have limited cycle life due to the oxidation/reduction process. Metal oxides and conducting polymers exhibit pseudocapacitance.[10,70]

EDLCs store charge electrostatically in an electrochemical double layer, which is formed at the electrode/electrolyte interface. As a major difference to pseudocapacitors and batteries, there are no redox reactions occurring. Thanks to this, there is no swelling of the material during charge/discharge cycles lengthening EDLCs cycle life. EDLCs also have high power density, as they have very fast charge and discharge cycles. They however have limited energy density due to the electrostatic surface charging mechanism.[9,11]

SC devices typically consist of an electrode material, a current collector, separator and electrolyte. Electrodes have electrochemically active material to store charge, and a current collector connect the electrodes to the external circuit. The separator separates the electrodes to avoid short circuiting, and the electrolyte carry and transport ions.[71] SC systems can be divided into symmetric SCs, asymmetric SCs and hybrid SCs. Symmetric SCs are made of two identical electrodes and asymmetric SCs have two different electrodes with one being a double-layer carbon material and the other being a pseudocapacitor material. Hybrid SC systems are instead composed of a SC-type electrode and a battery-type electrode.[11]

The electrolyte is an important part of the SC, as it can affect the capacitance, cycle life, power density and energy density. The electrolyte determines the operational cell voltage, and interactions between the ion and solvent can affect the lifetime of the SC. Liquid electrolytes used in SCs are organic electrolytes, aqueous electrolytes, ionic liquids. All electrolytes have their own advantages and disadvantages.[11,72,73] Organic electrolytes and ionic liquids can

operate at a higher voltage but can suffer from lower ionic conductivity. Organic electrolytes and ionic liquids usually require complex purification procedures in a strictly controlled atmosphere to avoid moisture. Aqueous electrolytes instead have high capacitance and conductivity, but have a limited working potential range due to water decomposition.[11,73] They are also inexpensive, and don't require special conditions simplifying the fabrication and assembly process[72]. Most popular aqueous electrolytes are H_2SO_4, KOH and Na_2SO_4[11].

Different carbon materials have been studied for SC electrode materials, such as activated carbon, porous carbon, carbon nanotubes and graphene. Carbon materials are studied for their abundance, non-toxicity, easy processing, high chemical stability, good electronic conductivity and high specific surface area.[9,74] Carbon materials are predominantly EDLCs[11]. Graphene-based materials have been studied for SC electrode materials, and as EDLCs they highly rely on high specific surface area between the electrode/electrolyte interface which can be disturbed by aggregation and poor wetting on the electrode surface.[75] With the addition of functional groups on the graphene structure, they can offer pseudo capacitance, as well as improve the wetting between the electrode and polar electrolytes[76]. For SCs the ideal structure of functionalized graphene would have an undisturbed conjugated system in the middle with functionalities on the edges.[75]

Common electrochemical studies for evaluating SCs are cyclic voltammetry (CV), galvanostatic charge/discharge (GCD) and electrochemical impedance spectroscopy (EIS)[11]. CV can be used to get insight into the charge-discharge mechanism of the material by applying a cyclic potential sweep and observing the current response. CV can also be used to evaluate the charge storage mechanism, if the resulting CV curve has a rectangular shape, it indicates EDLC behaviour, and redox peaks suggest pseudocapacitance.[77]

In a GCD measurement a constant current is applied to charge and discharge the material. Capacitance can be calculated from the duration of the charge/discharge, set current and change of potential. Additionally, the shape of the curve can suggest the type of capacitor behaviour as symmetric straight lines indicate EDLC behaviour, while triangular curves with small plateaus can indicate pseudocapacitance[77]

1.5 rGO-CNF composites

Often in composites rGO is combined with materials like conducting polymers, metal oxides or CNFs to avoid aggregation from occurring and simultaneously worsening the rGO's electrical properties.[78] In an rGO-CNF composite, CNFs enhance the mechanical strength and flexibility of the material as rGO by itself is stiff and brittle. The many -OH groups on CNFs surface offer hydrogen bonding sites that enable interactions between it and the rGO.[12]

rGO-CNF composites can be prepared as films, aerogels and hydrogels. rGO-CNF films can be prepared using vacuum filtration or chemical vapor deposition.3D materials can be prepared through freeze-drying or freeze-casting.[79]

rGO-CNF materials can offer versatility, as by varying the ratio of rGO to CNF the conductivity, the balance between conductivity and mechanical strength can be fine-tuned for different applications. Applications for rGO-CNF include energy storage, water filtration, flexible electronics, sensors and biomedical applications like drug delivery, tissue engineering and biosensors.[36,79]

When compared to currently employed SC systems, cellulose and rGO based SC systems have shown advantages with their low cost, flexibility, environmental friendliness and versatility. Thin films are the most common structure of rGO-CNF composite for SC applications.[78] Both rGO and CNF also have high surface area, and in the composite CNFs can help to offer diffusion channels for the electrolyte to promote the connection between the electrode and electrolyte, enhancing the electrochemical performance[13]. The challenges in rGO-CNF composites for SC application are high internal resistance as well as figuring out how to control the morphology, structure and distribution. Another focus for future research is how to simplify the composite production process.[78]

1.6 The objective

The objective of this project is to produce a self-standing rGO-CNF film for SC application with good electrical properties using green reduction methods with a simple production process. rGO is chosen for its conductivity, light weight, high specific surface area and

relatively low cost. As rGO itself is a brittle material, CNFs are added as an environmentally friendly way to enhance the mechanical strength of the resulting composite. CNFs can also prevent agglomeration to boost the electrochemical performance of the rGO-CNF composite compared to just pure rGO.

With the main focus on the hydrothermal reduction method, the first step is to find the ideal combination of reaction conditions for the best possible conductivity of the material using different temperatures, reaction times and pH. Chemical reduction using $NaBH_4$ and microwave reduction is also used to compare the different methods. To ensure the reduction has occurred, UV-Vis spectroscopy is used. The rGO suspension is also used to craft electrodes for a symmetric cell set up, then CV and GCD tests are used to study the electrochemical performance of the material.

After the reduction process, the CNFs are added via a simple sonication process. Electrodes are crafted in the same way as for the rGO, and CV and GCD studies are done. Additionally, films are made using vacuum suction filtration, which are then studied using 4-probe conductivity measurement as well as XRD.

2 Experimental section

2.1 Materials

Table 1 shows the materials and chemicals used in the project and their manufacturers.

Table 1. Materials used in the project and their manufacturers

Material	Manufacturer
Graphene oxide dispersion (5 mg/mL)	UTU
Nafion 5%	Sigma-Aldrich
Sulfuric Acid (H_2SO_4, 1 mol/L)	Merck
Graphite sheet	Thermo scientific
Ethylene Glycol	TCI
N-Methyl-2-Pyrrolidone	TCI
Sodium borohydride	Merck
0.1 µm PC membrane 47 mm hydrophilic	Isopore
High charge TEMPO oxidized cellulose nanofiber hydrogel (0.93%)	Prof. Chunlin Xu & Dr. Xiaoju Wang, Åbo Akademi University
Cellulose nanofiber hydrogel (1.7%)	Asst. Prof. Jaana Vapaavuori, Aalto University

2.2 Instruments

Table 2 shows the equipment used in the project.

Table 2. Equipment used in the project

Instrument	Manufacturer
Ultrasonic cleaner USC-THD	VWR
High pressure reactor 4593	Parr
Parr reactor controller 4848	Parr
UV-Vis spectrometer Cary 60	Agilent
X-ray powder diffractometer	PANalytical Aeris
Potentiostat	Autolab
Centrifuge Biofuge stratos	Heraeus
Centrifuge	Sigma
Rotavapor	Heidolph
Microwave Synthesizer Discover	CEM

2.3 Reduction of GO

2.3.1 Hydrothermal reduction

Hydrothermal reduction was done using the Parr high pressure reactor. The set up consists of the reactor chamber with a Teflon liner and a built-in stirrer, as well as a heater and a reactor controller to set the temperature. N_2 gas can be added into the reactor through a tube to increase pressure, and the reactor is also equipped with a sampling tube to remove the sample without shutting down the reactor. The high-pressure reactor and controller are presented in figure 4, and the reaction vessel, Teflon liner and the temperature probe, sampling tube and stir bar in figure 5.

Notably, while the temperatures used for hydrothermal reduction are shown as one value, in reality, it the deviates with 1 – 5°C from the setpoint due to fluctuation caused by the method of heating that the reactor uses. The heater outside seems to heat the reactor based on the reading of the temperature probe inside the reactor, surrounded by the liquid and Teflon liner. Due to this the sleeve reacts with a delay, causing the fluctuation.

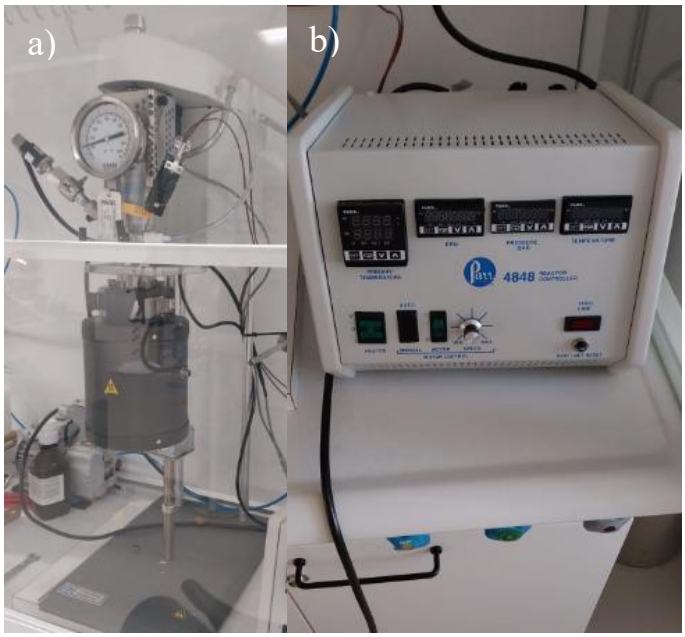

Figure 4. a) The high-pressure reactor b) The reactor controller.

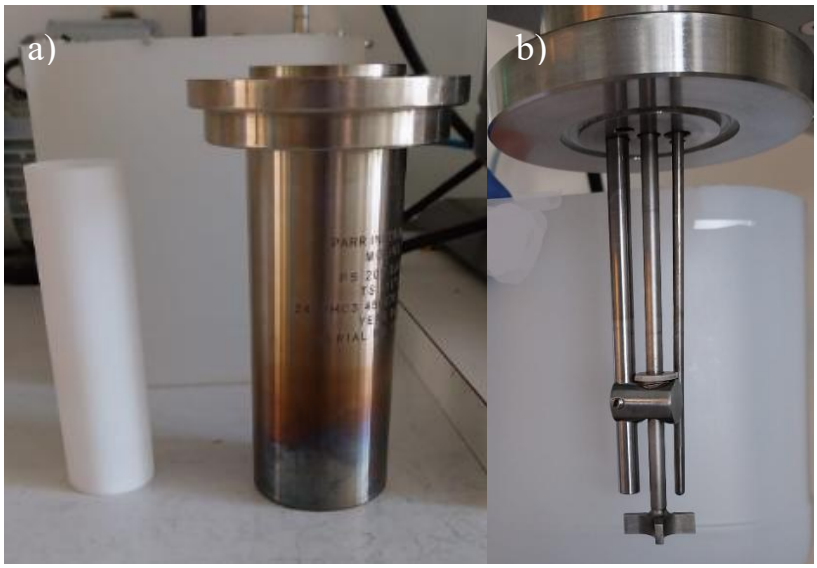

Figure 5. a) The Teflon liner and reactor chamber b) The sampling tube, stir bar and temperature probe.

Samples prepared using the hydrothermal method are coded with the letter H and a number (H1, H2 etc.). The general process is explained here, and the specific details for each sample are listed in table 3.

Before reduction, GO suspension and DI water are combined. One sample is done using EG instead (while this makes it more of a solvothermal reduction it is included for simplicity in the hydrothermal section). If sonicated, it is done before loading the sample into the reaction vessel. pH can be adjusted if desired, and pH is measured before reduction. The vessel is closed air tight and degassed to remove oxygen using N_2. N_2 is added until a pressure of 7 bar is reached, and the solution is stirred at 650 rpm for 5 min. The gas is then released and this is repeated 3 times.

After degassing, pressure can be added into the reactor for the reduction reaction. The GO solution inside is stirred at 650 rpm, and the heating is turned on while observing the pressure build up. The reaction time is started once the required temperature is reached and stabilized.

Some of the sample can be removed through the sampling tube during the reaction by stopping the stirring for the duration. After the full reaction time is completed, the heater is removed and the stirring is stopped. The reactor is cooled down with ice, and once room temperature is reached the pressure is let out.

After the sample is removed from the reaction vessel, its pH is measured and it is then washed to reach a neutral pH. This is done by centrifuging the rGO suspension, decanting the liquid and adding new DI water. This is repeated until the desired pH is reached.

Table 3. Sample preparation and reaction details used for hydrothermal reduction.

Sample	GO (mg)	GO (mL)	DI (mL)	c (mg/mL)	pH pre-reduction	Sonication (min)	Added P (bar)	t (h)	T (°C)
H1	10	2	50	0.2	6	-	7	1	80
H2	50	10	40	1	6	-	7	3	120
H3	25	5	60	0.4	6	-	7	6	120
								+18(24)[c]	120
H4	50	10	40	1	9[a]	-	7	3	120
								+6 (9)	120
								+3 (12)	150
								+6 (18)	180
H5	50	10	40	1	6	30	-	3	180
								+3 (6)	180
H6	50	10	40	1	6	30	7	6	220
H7	50	10	40	1	6	30	7	24	120
H8	50	10	10	2.5	4	30	7	6	120
H9	10	2	20 (EG)[b]	0.45	7	30	-	1	140
								+2 (3)	140

[a] pH adjusted using NH_4OH, [b] Ethylene glycol added instead of DI water, [c] same sample continued for 18 h making total reduction time 24 h

2.3.2 Chemical reduction

Chemical reduction is done using $NaBH_4$. Samples reduced using the chemical method are titled with the letter C and a number. Chemically reduced samples are washed the same way as the hydrothermal samples.

Rotavapor reduction

10 mL of GO dispersion is combined with 100 mL of DI water and sonicated for 30 min in a round bottom flask. The desired amount of $NaBH_4$ is weighed and added to the GO solution, washing the residual $NaBH_4$ from the weighing boat with a small amount of DI water. The reduction is done using a rotavapor at 80°C for 1h, using minimal vacuum with the bottle spinning slowly. After the 1h reduction time the vacuum and spinning speed is increased to evaporate water until < 50 mL is left. The reduction details are presented in table 4, and the rotavapor used is presented in figure 6.

Table 4. Reduction details for chemical reduction

Sample	GO (mg)	GO (mL)	DI (mL)	c (mg/mL)	pH	sonication (min)	ratio (GO:R)[a]	$NaBH_4$ (mg)	t (h)	T (°C)
C1	50	10	100	0.45	6	30	1:7	378	1	80
C2	50	10	100	0.45	6	30	1:10	500	1	80

[a] ratio of GO to reducing agent based on weight

Figure 6. The rotavapor used for chemical reduction.

Sonochemical reduction

For sample C3 a combination of sonication and chemical reduction was used. 2 mL of GO dispersion was sonicated in a sealed glass vial for 2h making sure the sonicator's temperature stays below 25°C. After this, 100 mg of $NaBH_4$ was added into the vial, which was then resealed. Finally, the solution was sonicated for 1h more, again keeping the temperature below 25°C.

2.3.3 Microwave reduction

Microwave reduction was done using the CEM Microwave synthesizer Discover. Special microwave vessel was used, equipped a lid which can release pressure as well as a magnetic stir bar for mixing during the reaction. All samples were stirred by the synthesizer for 2 min before starting.

Reaction parameters include temperature, ramp time, hold time, pressure and power. Ramp time is the time excluded from the reaction time, meant to heat the reactor. Hold time is the time the set temperature is kept stable for the reduction process. Details for each sample are listed in table 5 below.

Table 5. Reduction conditions set to use in microwave reduction

Sample	GO (mL)	GO (mg)	Added solvent	Solvent (mL)	c (mg/mL)	T (°C)	Ramp time (min)	Hold time (min)	Pressure (psi)	Power (W)
M1	1	5	-	-	5	25	1	10	200	300
M2	1	5	-	-	5	120	3	30	200	300
M3	1	5	DI	1	2.5	160	3	30	200	300
M4	1	5	DI	1	2.5	200	5	60	200	300
M5	0.5	2.5	DI	0.5	2.5	230	8.5	30	200	300
M6	1	5	NMP	1	2.5	230	30	150	200	300

2.4 Preparation of rGO-CNF composite

Composites were prepared from GO in a 50:50 ratio based on weight (dry weight of CNF). The CNFs used are High Charge TEMPO oxidized CNF hydrogel from Åbo Akademi University, and CNF hydrogel from Aalto University. These were supplied to us and were

used without any pre-treatment. The rGO used in the composites was the highest performing hydrothermally reduced one.

The composites are prepared with 10 mg of rGO. For 10 mg of dry weight CNF, the required amount of hydrogel was calculated. For rGO-CNF-1, no DI water was added to the rGO and 4.4 mL of DI water was added to the CNF to make a composite with a total volume of 10 mL. For rGO-CNF-2 and rGO-CNF-3, 4.4 mL of DI water was added to the rGO, and 10 mL was added to the CNF to make the composites total volume 20 mL. Water is added because from previous experiments we learned that adding DI water to the CNF hydrogel before sonication helps to break down the gel clumps and results in a more uniform composite.

The rGO and CNF are sonicated separately for 15 minutes in closed conical flasks. The CNF is poured into the rGO, and the residue is washed with a small amount of DI water. After combining they are sonicated for 1 h, keeping the sonicator's temperature below 25°C. Details of the process are presented below in table 6.

Table 6. Details of composite preparation.

Composite	m(rGO) (mg)	V(rGO) (mL)	DI to rGO (mL)	CNF type	Hydrogel m%	m(CNF hydrogel) (mg)	m(CNF dry) (mg)	DI to CNF (mL)	V(total) (mL)
rGO-CNF-1	10	5.6	-	HC TEMPO[a]	0.93	1.08	10	4.4	10
rGO-CNF-2	10	5.6	4.4	HC TEMPO	0.93	1.08	10	10	20
rGO-CNF-3	10	5.6	4.4	Aalto CNF[b]	1.64	0.61	10	10	20

[a] High charge TEMPO oxidized cellulose nanofiber hydrogel from Åbo Akademi University [b]CNF hydrogel from Aalto University

2.5 Preparation of electrodes

Electrodes were prepared on graphite foil. The foil was cut into 1cm wide strips and covered with tape to eliminate the foil from reacting with the electrolyte, leaving a 1 cm^2 area uncovered for drop casting (Figure 7).

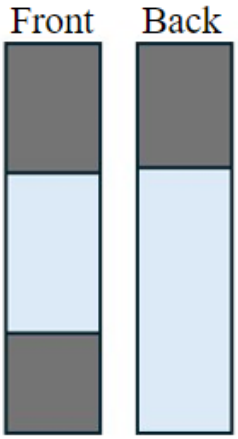

Figure 7. Schematic of the electrodes with the tape placement in blue.

Coating method

For preparing two electrodes, a volume containing 2 mg of rGO in DI water was sonicated in a glass vial for 30 min. For composites the sample also contains CNF hydrogel. The sample was then drop casted onto the grafoil in 100 µL layers, which were then dried in an oven at 100°C. This was repeated until 1 mg/cm^2 was reached on each electrode. Before the last layer had dried, 5 – 10 µL of Nafion (5%) was dropped onto the electrode.

Ink method

While otherwise identical to the coating method, in the ink method Nafion is added into the glass vial together with the sample, which are then sonicated together for 30 min.

The details on electrode preparation for each sample are presented in the supplementary section, in table S1.

2.6 Conducting film preparation

Films were prepared using vacuum filtration, using a filtration funnel with base equipped with a sintered disc for uniform filtration. The membrane is placed between two rubber rings, which in turn are placed between the funnel and base. The parts are then clamped together. The set up is presented below in figure 8.

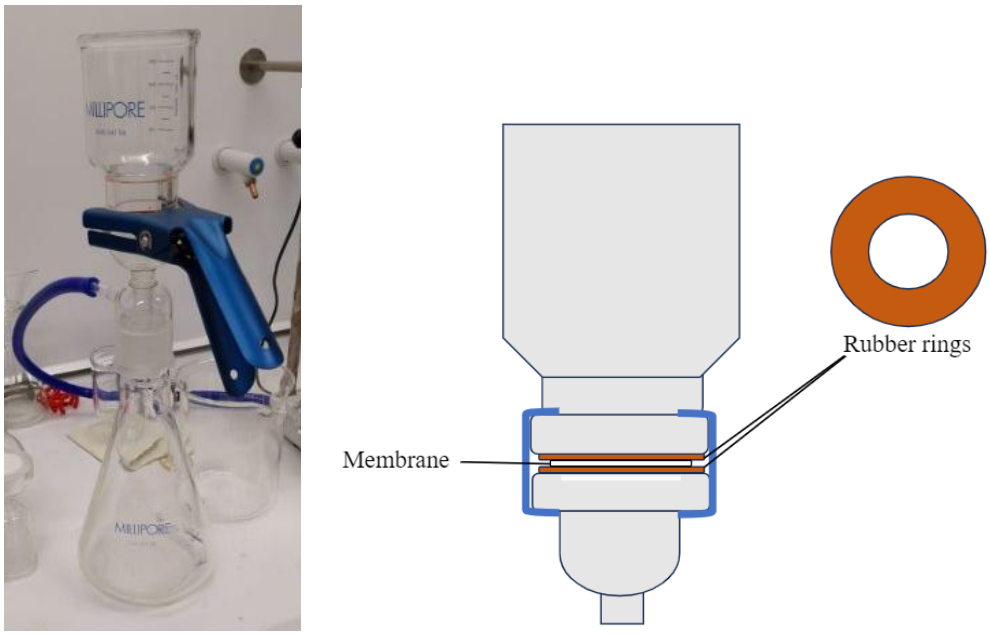

Figure 8. Suction filtration set up.

Using hydrophobic 0.1 µm PC membranes, a volume containing 5 mg of rGO of the sample is filtrated through until a "wet cake" formed. After this, the membrane with the sample on it is removed and left to dry overnight in room temperature under a weight pressing down the edges to prevent curling. After drying the film was peeled off the membrane.

2.7 Materials characterization

2.7.1 UV-vis spectroscopy

Ultraviolet visible (UV-vis) spectroscopy is based on the interaction between chemical species and light in the UV-vis spectrum. In characterization of rGO, UV-vis spectroscopy can be used to gain qualitative insight into the reduction method's effects. The UV-vis spectra of GO show an absorption peak maxima at around 230 nm which corresponds to the $\pi - \pi^*$ transition of aromatic C-C bonds. In rGO, the pi bond conjugation is increased after reduction which can then be identified as a red shift of the UV spectra, and the maximum absorption peak of rGO is around 265 nm.[4]

UV-Vis measurements were done using a quartz cuvette, and an example spectra is presented in figure 9 showing the peak positions of GO and rGO.

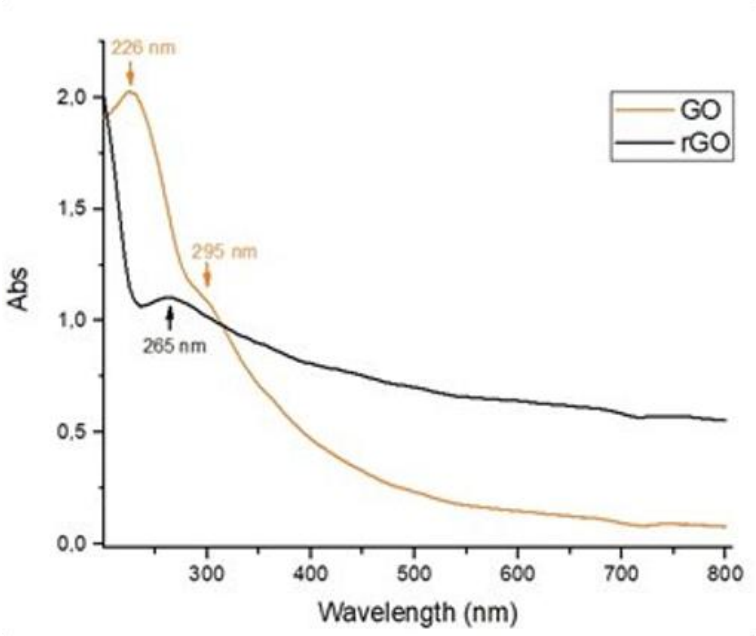

Figure 9. UV-Vis spectra of GO and rGO showing their characteristic peaks.

2.7.2 X-ray diffraction spectroscopy

X-ray diffraction (XRD) can be used to identify the elements in a sample and study the crystallinity, crystal orientations and phases of the sample. XRD is based on Bragg's law, and is a non-destructive characterization method. During an XRD measurement a monochromatic beam of X-rays is directed at the sample, and the reflected X-rays are then collected by the detector. Amorphous materials produce a broad peak, and crystalline materials produce sharp peaks.[80]

XRD can give insight into the reduction process as GO shows a peak at around 10° and rGO at around 23-24°[51]. CNFs main diffraction peaks instead are located at approximately 16° and 23°[81]. XRD was done on two thin films that were prepared from two different CNFs using a Cu Kα source using the fast scan mode, using a silicone substrate

2.7.3 Conductance tests

The 4-probe conductivity measurement can be used to study the electrical properties of thin films by measuring the conductivity/resistivity of the material. It uses four probes arranged in

a line which are lowered onto the surface of the tested material. The outer probes are used to inject a current from a current source, and the inner two probes measure the voltage.[82]

4-probe conductivity measurements were done on the films. The set up is presented in figure 10. During the test the film is placed on a glass slide to have a nonconducting base, and pressed with the 4, with a potential window from 0 – 1 V.

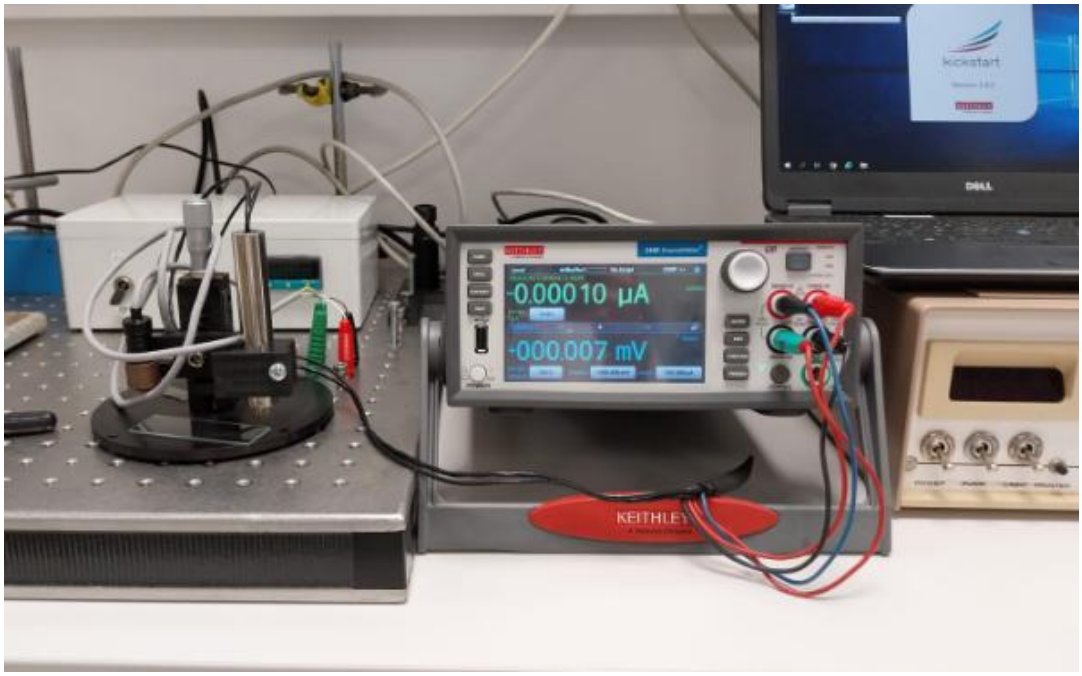

Figure 10. 4-probe conductivity measurement set up.

2.8 Electrochemical measurements

Electrochemical measurements were done on the electrodes to measure their electrochemical performance using Autolab Potentiostat, equipped with the NOVA 2 program. Blank grafoil electrodes were also tested for comparison. The electrochemical cell used in the measurements was assembled into a symmetrical two-electrode set up (figure 11), with 1M H_2SO_4 as the electrolyte. In a two-electrode set up the working electrode (WE) is connected to one of the electrodes, while the reference electrode (RE) and counter electrode (CE) are connected to the other. Before measurements the electrolyte was purged with N_2.

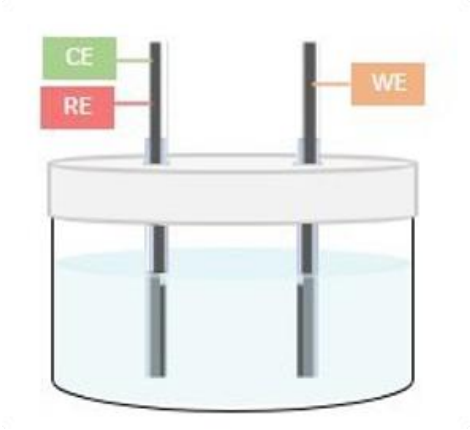

Figure 11. Schematic of the 2-electrode symmetric electrochemical set up using grafoil electrodes with the WE, CE and RE placements shown.

Cyclic voltammetry measurements were conducted using a scan rate of 50 mV/s and a potential window between 0 – 1 V. Galvanostatic charge-discharge measurements were done with different current densities: 0.25 A/g, 0.5 A/g, 1 A/g, 2 A/g, 3 A/g and 5 A/g. The potential window for the GCD was between 0 – 1 V for 5 cycles. Areal and Specific capacitances for symmetric two-electrode set up were calculated from the GCD measurements using the equations presented below.

$$C_a = \frac{2 \times I \times \Delta t}{(\Delta V - IR)} \quad (1)$$

Where C_a is the areal capacitance (F/cm^2), I is the current (A), Δt is the discharging time (s), ΔV potential window (V) out of which the IR drop is subtracted.

$$C_p = \frac{2 \times I \times \Delta t}{m \times \Delta V} \quad (2)$$

Where C_s is the specific capacitance (F/g), I is the current (A), Δt is the discharging time, m is the mass of active material on one electrode (g) and ΔV is the potential window (V).

3 Results

Hydrothermal reduction

Calculated amounts (Table. 3) of GO starting material was reduced in hydrothermal condition using Parr autoclave reactor. When GO was reduced it goes through a colour and consistency change that can be seen with just the naked eye. While GO was a homogeneous brown liquid, after reduction it turned into individual black particles dispersed in a clear water liquid (Figure 12).

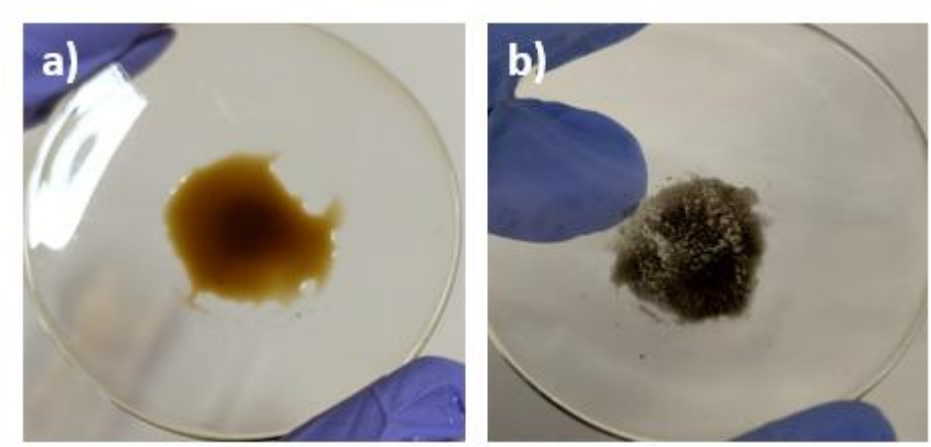

Figure12. a) GO suspension b) rGO in water.

The pH of most samples changed to slightly more acidic during the reduction, with samples starting at pH 6 with a final pH of 5. The basic pH of sample H4 stayed at pH 9, and the EG sample H9 stayed at pH 7. Sample H8 with a higher concentration remained at pH 4. The pressure inside the reactor depended on the temperature used, and if external pressure (N_2, 7 bar) was added into the reactor before reduction. These are presented in the supplementary in table S2.

For sample H6, the synthesized sample was collected fully through the sampling tube in the autoclave reactor, to avoid the rGO from possibly being affected by the cooling of the reactor which took 30-60 min depending on the reaction temperature. Removing sample through the sampling tube however caused most of the dispersion to be removed, but most of the rGO got stuck and dried on the walls of the reactor, resulting in the concentration of the rGO dispersion to be very low and no electrodes were made using this sample (Figure 13).

Figure 13. Sample H6 with hardly any rGO in it.

Using the hydrothermal method GO was reduced (turned black) which occurred in neutral / acidic pH at 3h in 120°C. Lower temperature and shorter time didn't turn the GO into black dispersion, indicating reduction had not occurred. The solvothermal method used for H9 didn't yield in reduction, until 3h at 140°C. In the sample H4-rGO, the pH was adjusted to 9, and it took longer time for the reduction to take place compared to neutral / acidic pH medium. The sample didn't turn black until a total reduction time of 18h with temperatures increased up to 180°C. Figure 14 shows a partly reduced H4 with black particles but still some brown colour can be seen indicating a partial reduction.

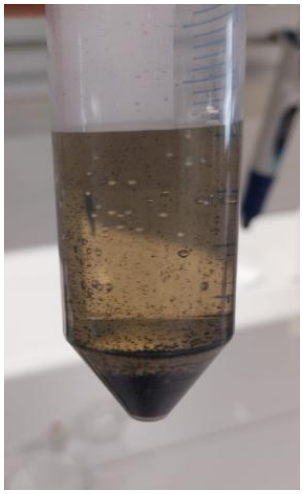

Figure 14. Partially reduced H4 sample with some black particles.

Hydrothermally reduced samples have a "fluffy" consistency right after reduction, and during overnight some of the rGO particles sinks to the bottom of the collection tube, while some particles stay floating and stick to the side wall (Figure 15).

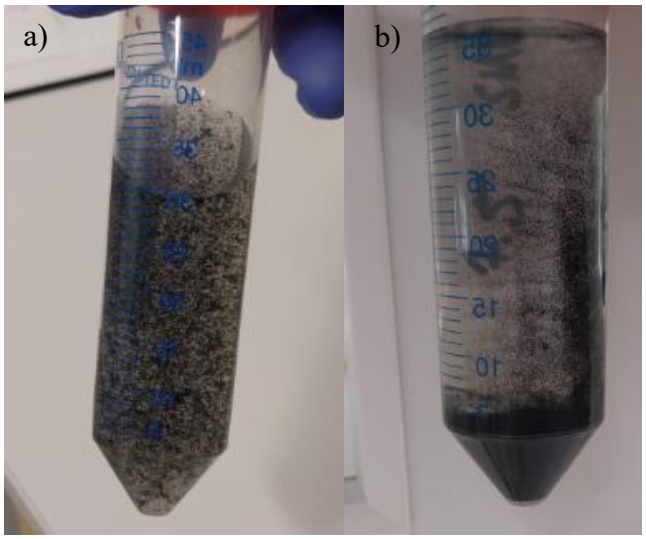

Figure 15. Hydrothermally reduced sample a) right after reduction and b) after overnight aging.

Chemical reduction

All chemically reduced GO samples turned into black (rGO), and the pH after reduction for C1 was 9, and for C2 and C3 the pH was 10. After leaving the sample overnight for aging, the rGO particles allowed to settle at the bottom of the tube (Figure 16).

Figure 16. After chemical reduction, all rGO particles settle at the bottom.

Microwave reduction

While you can set a desired temperature and time etc. the microwave synthesizer has limits on what it can do. For example, to reach 160°C a ramp time of 3 min was not enough, and 5 min

of the hold time went into heating the vessel to reach the temperature, resulting the actual hold time to be 25 min.

While the power was set to the max (300 W), the power would stay at maximum only until the set temperature was reached, at which point the power would get lowered to maintain that temperature. Only if the temperature was set at 220 – 230°C the power stayed at 300 W for the entire duration of reduction process. The actual reaction times and temperatures that happened during the reduction are presented in table 7.

Additionally, the reactor doesn't hold the pressure, and no added pressure was applied during the reduction other than the autogenic pressure (<20 psi) created during the initial heating process. This pressure also got released during the process through the loosely attached lid.

Table 7. The actual hold times, temperatures and power at which the samples were reduced in.

Sample	Actual hold time[a] (min)	Actual T[b] (°C)	Power during reduction[c] (W)
M1	10	36	0
M2	30	120	100-120
M3	25	160	130-160
M4	45	200	200
M5	-[d]	220	300
M6	120	230	300

[a]The reduction time after the set temperature was reached, [b]the actual temperature during reduction, [c] the power that was on during the hold time, [d] the set temperature (230°C) was not reached during the experiment

Even just based on the colour, we could able to recognize that the samples M1 and M2 didn't reduce and remained a brown coloured (GO) liquid (Figure 17a), and M3 was only partially reduced with some black particles (Figure 17b) dispersed, but still had brown colour in it.

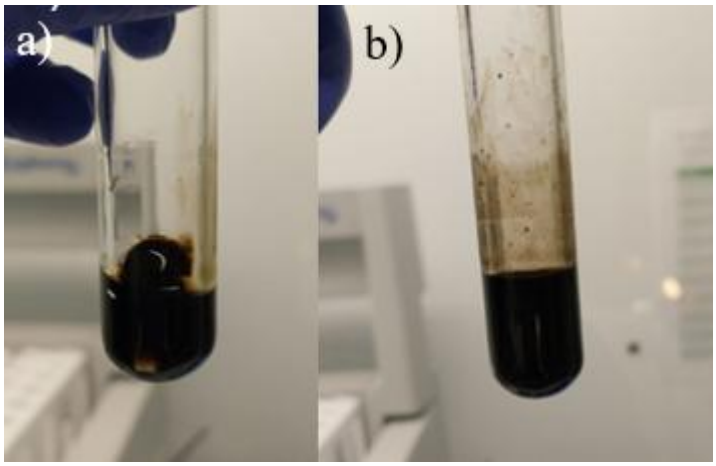

Figure 17. a) Sample M1 still brown after microwave treatment b) Sample M2 remained mostly brown with some black particles.

Samples M4-M6 were reduced (turned black). Overnight, some of the rGO particles sank to the bottom and some floated to the top of the centrifuge/collection tube (Figure 18) indicating different sized rGO particles/flakes. The variability in particle size can also be seen in Figure 19 with visible clumps.

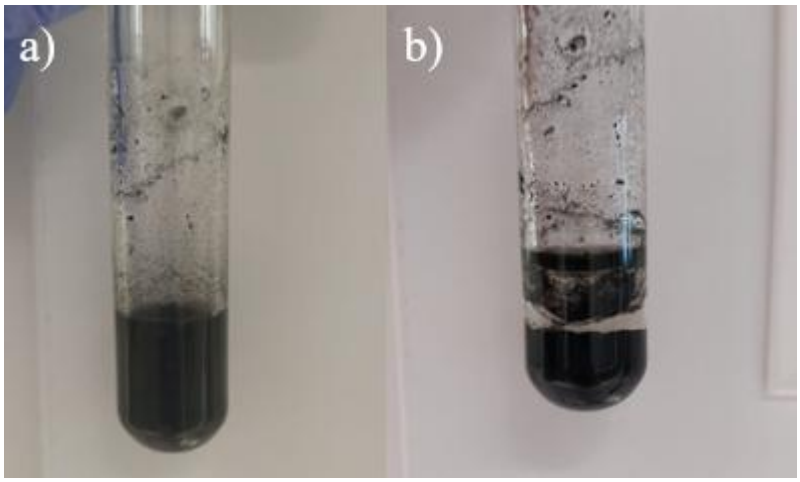

Figure 18. a) Sample M5 right after reduction b) Sample M5 the next day.

Figure 19. Consistency of sample M5 with visible larger clumps of rGO.

Composite

Comparing the consistency of the different composites we could tell adding DI water helped to break down the CNF clumps and make a more homogeneous mix with the rGO particles. Compared to the rGO, the composite is more viscous and has a more homogeneous look overall with the particles suspended in the liquid and not sinking to the bottom of the collection tube (Figure 20).

Figure 20. The consistency of the rGO-CNF composite.

Film preparation

Films were prepared from the composites using the aforementioned method and were successfully removed from the supporting membrane. Another film was prepared from just rGO, which was not possible to remove from the membrane without ripping. (Figure 21) The composite films were thicker and had flexibility, showing the CNF enhanced the mechanical strength and elasticity of the film.

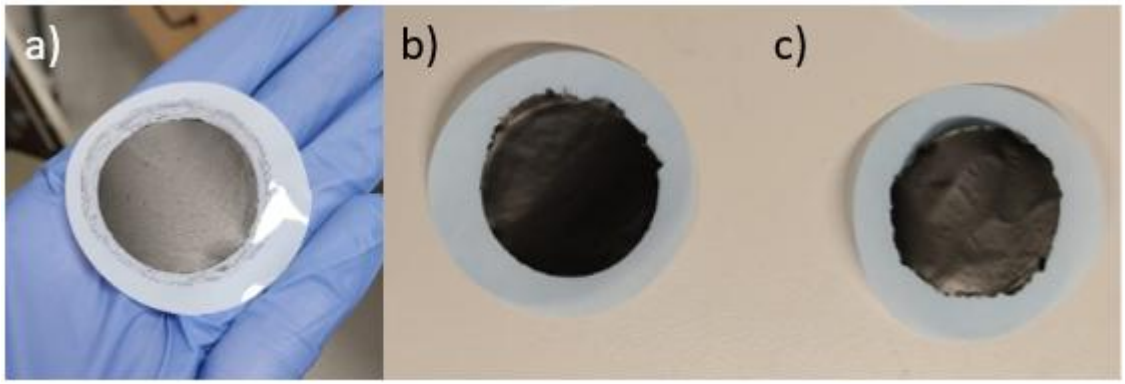

Figure 21. a) Film prepared from rGO alone, stuck on the membrane, and films prepared from composites b) rGO-CNF-2 and c) rGO-CNF-3.

3.1 Materials characterization

3.1.1 UV-Vis spectral data

Hydrothermal reduction

From the UV-Vis spectra in figure 22 below, we can see that when GO was reduced for 3h in 120°C there was a peak at 255 nm, and after 6h in 120°C there was a peak at 260 nm showing a small shift to the right, possibly indicating a more thorough reduction. Similarly, the GO sample reduced for 6h in 180°C shows a very subtle curve at the 265 nm mark. All samples that were reduced for 18 – 24h show a flat line, with no peaks visible. These samples might be over processed, and was closer to graphite than rGO.

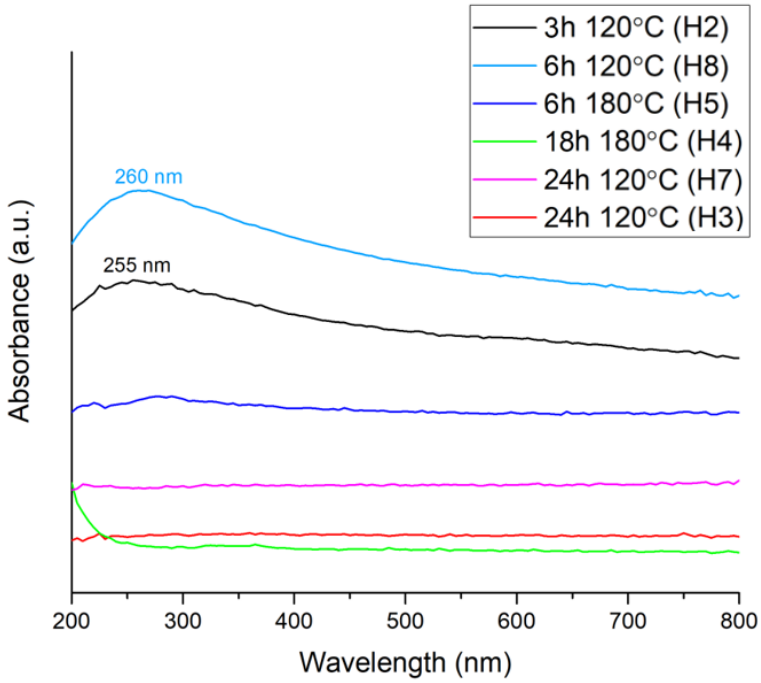

Figure 22. UV-Vis spectra of hydrothermally reduced samples, showing the rGO peak flattening in harsher conditions.

In figure 23 below, the UV-Vis spectra shows that the H9 sample that was reduced in EG has a peak at 235 nm. This might indicate that the sample wasn't fully reduced, and still has GO in it.

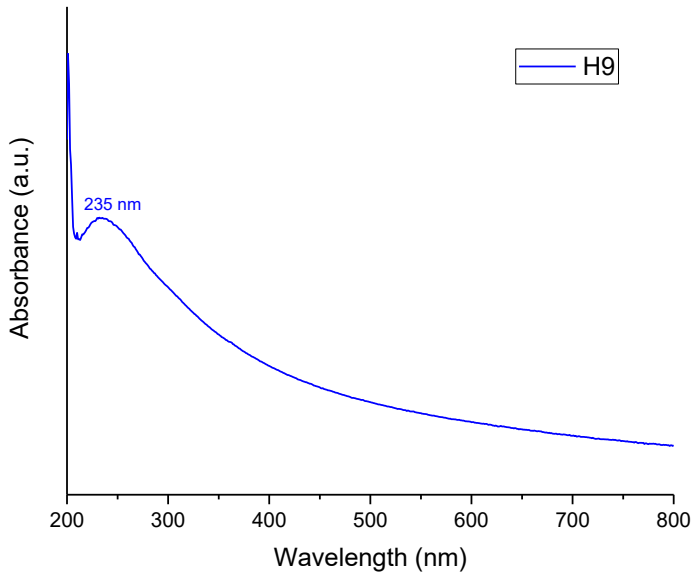

Figure 23. The sample reduced in EG shows a peak at 235 nm.

Chemical reduction

All three chemically reduced GO samples show a single peak at 265 nm, presented in the UV-Vis spectra in figure 24.

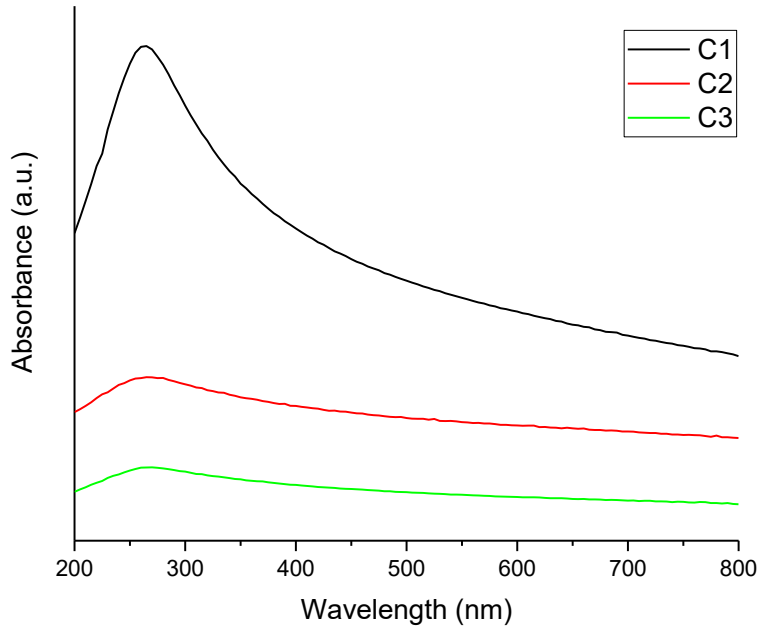

Figure 24. The UV-Vis spectra of chemically reduced samples showing a single peak at 265 nm.

Microwave reduction

The microwave reduced samples M4 and M5 show peaks at 255 nm and 260 nm, respectively, showing the GO has been successfully reduced. Between M4 and M5, a small shift to the right can be seen. M6 was reduced in NMP, which could not be washed away from the sample and thus the possible rGO peak is covered by NMP's absorbance (Figure 25).

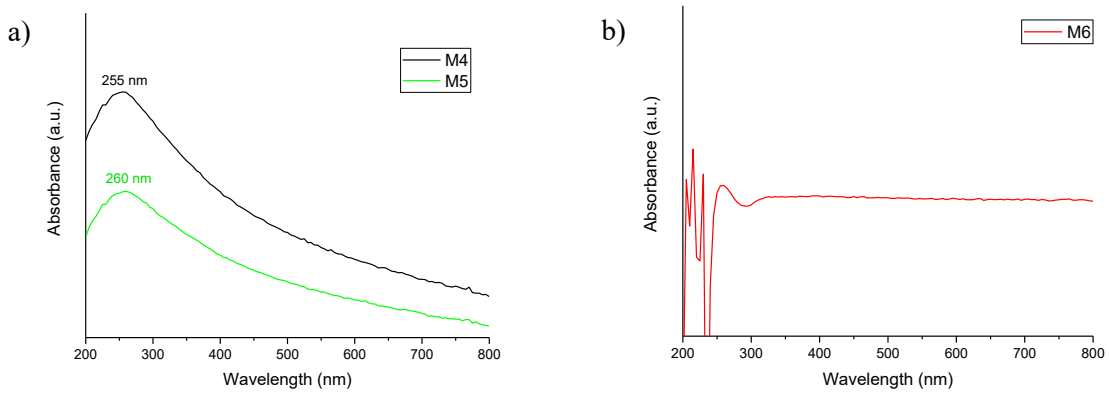

Figure 25. a) UV-Vis spectra of the microwave reduced samples b) UV-Vis spectrum of sample M6 reduced in NMP, with the possible peaks covered by NMP's absorbance.

Composite

UV-Vis measurements were also done on the composites, showing nearly identical spectra for all three samples, with only the rGO peak visible at 265 nm showing the rGO has not been affected by the cellulose's presence, when preparing the composite (Figure 26).

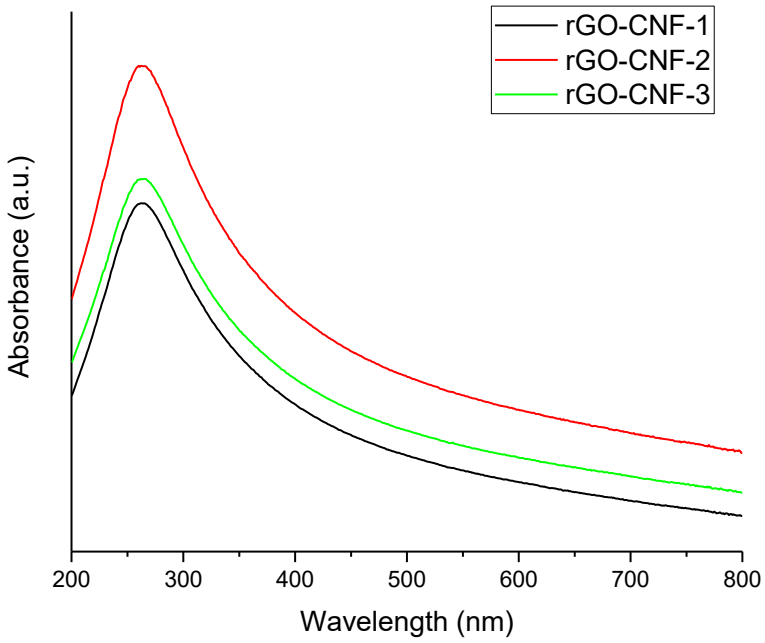

Figure 26. UV-Vis spectra of the rGO-CNF composites.

3.1.2 XRD spectral data

XRD graphs of rGO-CNF-2 and rGO-CNF-3 are mostly similar, but rGO-CNF-3 showed some more distinct peaks revealing some crystallinity in the structure. With no peaks at around 11°, we can further conclude that no GO was present and has been fully reduced. rGO and CNF peaks overlapped at the peak at 23° with a broad peak at 16° (Figure 27).

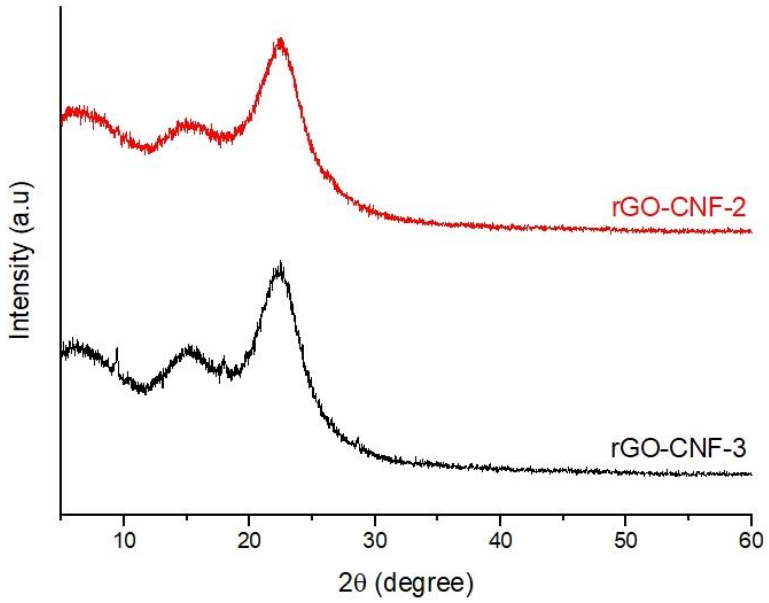

Figure 27. XRD patterns of rGO-CNF-2 and rGO-CNF-3.

3.1.3 Conductance tests results

For the conductance measurement, two films were compared, with rGO-CNF-2 showing a higher response than rGO-CNF-3. 4-probe conductivity measurements were also done on the film to check uniformity, with similar values being achieved when tried at different parts of the film for rGO-CNF-2, but some differences could be seen for rGO-CNF-3 (Figure 28).

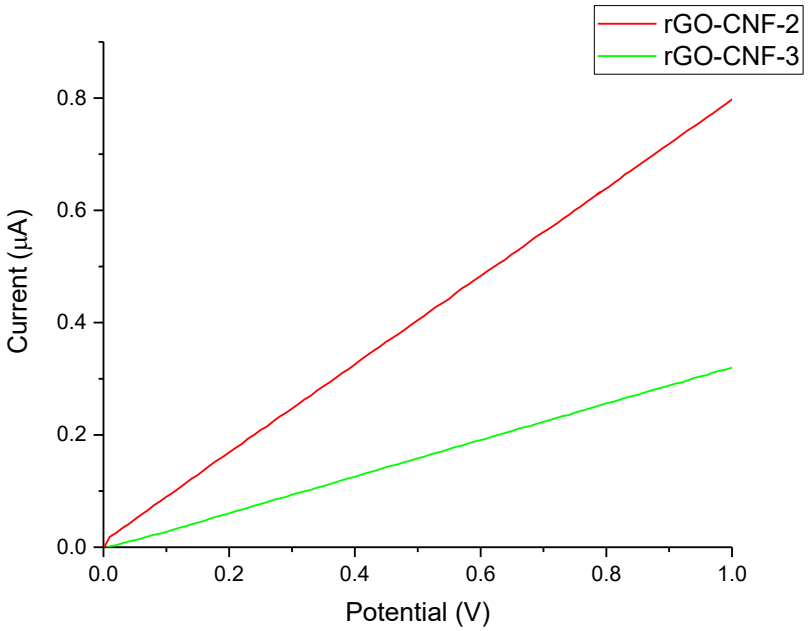

Figure 28. 4-probe conductivity measurements of the rGO-CNF-2 and rGO-CNF-3 films.

3.2 Electrochemical measurements

To see if the graphene foil shows conductance, a blank electrode was tested. Electrodes were also prepared using GO suspension. While the graphene foil shows some capacitance, the GO electrodes are close to zero at a capacitance of 2.9 F/g calculated from the GCD (Figure 29).

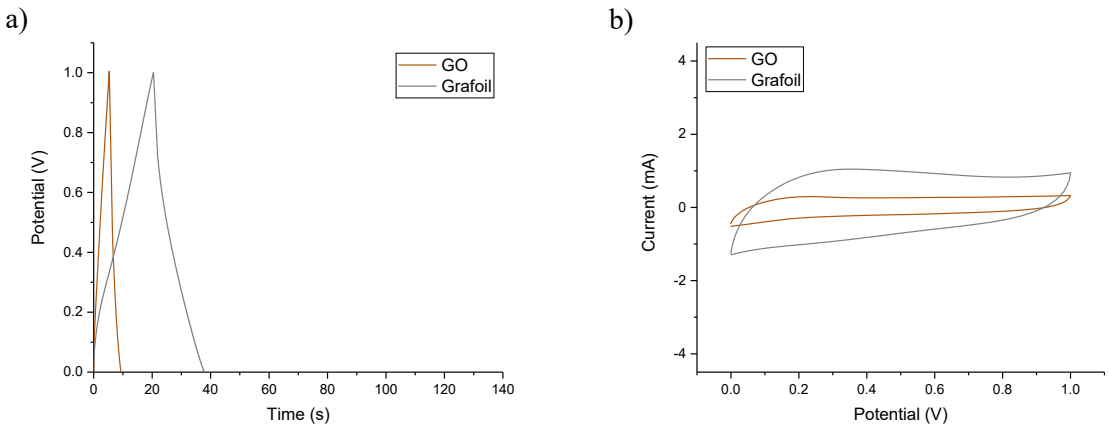

Figure 29. a) GCD plots of blank grafoil electrodes and electrodes coated with GO at 1 A/g in 1 M H_2SO_4 b) CV plots of blank grafoil electrodes and electrodes coated with GO using a scan rate of 50 mV/s in 1 H_2SO_4.

Sample load tests for the electrodes were done using different mass loadings (1 mg/cm^2, 2 mg/cm^2 and 3 mg/cm^2) to determine the ideal amount of rGO to be used on the electrodes based on specific capacitance (Figure 30)

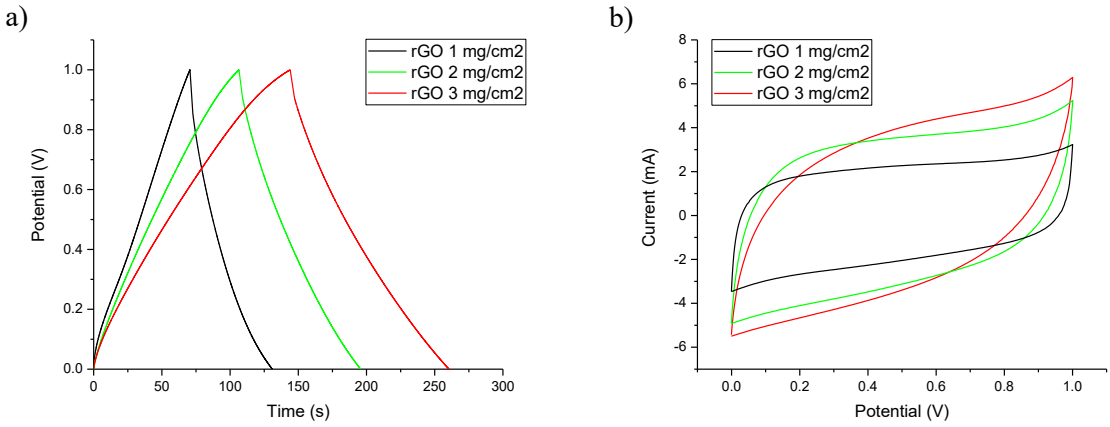

Figure 30. a) GCD plots of electrodes with different loadings at 1 A/g in 1 M $H_2SO_4$and b) CV plots of electrodes with different loadings using scan rate of 50 mV/s in 1 M H_2SO_4 electrolyte

Table 8. Specific capacitances of electrodes with different rGO mass loadings.

Loading (mg/cm^2)	**C_s (F/g)**
1	116.5
2	89.2
3	75.1

Different electrode preparation methods were compared using the same sample (1 mg/cm^2). Electrodes were prepared using coating and ink method to determine if it had effect on the electrochemical performance of the electrodes. From the GCD and CV measurements the ink method resulted in a higher capacitance than the coating method, at 94.3 F/g and 66.9 F/g respectively (Figure 31).

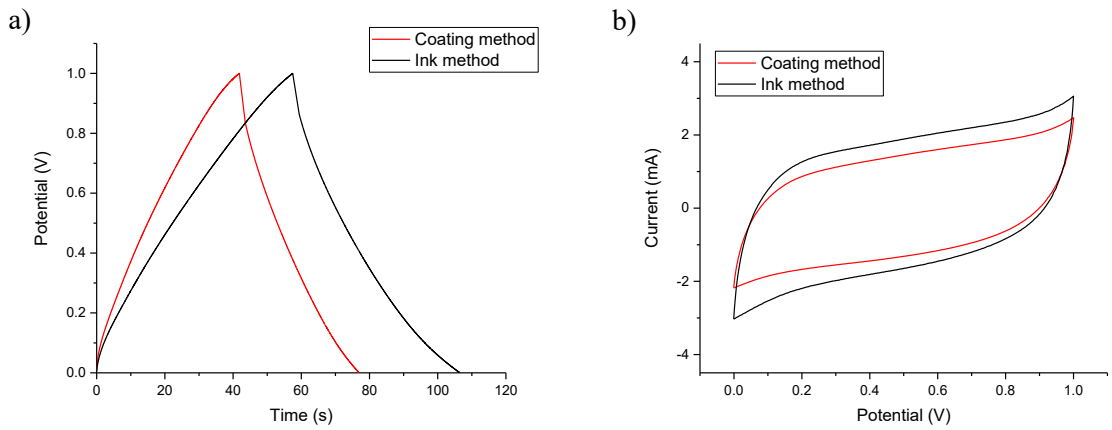

Figure 31. a) GCD plots of rGO electrodes prepared from the same sample using different preparation methods at 1 A/g in 1 M H_2SO_4 b) CV plots of rGO electrodes prepared from the same sample using different preparation methods in 1 M H_2SO_4at a scan rate of 50 mV/s.

Hydrothermal reduction

The effects of reduction time were compared using rGO samples reduced in the same conditions for 3h, 6h and 24h samples (H2, H8, H3). From the electrochemical studies it can be seen that the capacitance increases as the reaction time goes from 3h to 6h, but if continued to 24h the capacitance drops (Figure 32).

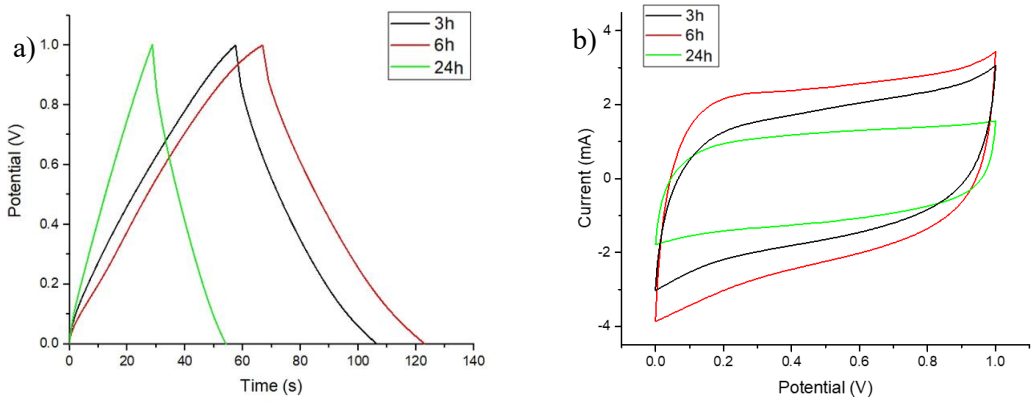

Figure 32. a) GCD plots of rGO samples reduced for different time durations in 1 M H_2SO_4 at 1 A/g b) CV plots for rGO sampled reduced for different time durations in 1 M H_2SO_4 at a scan rate of 50 mV/s.

The effect of sonication was also studied. From figure 33 below it is evident that sonicating the GO sample before reduction results in slightly higher capacitance (samples H5 6h and H8). Also, comparing a sample that was reduced first for 6h and then continued for 18h the next day (H5 24h) to a sample that was reduced continuously for 24h (H7) shows that it is better to reduce the sample in one go (Figure 33).

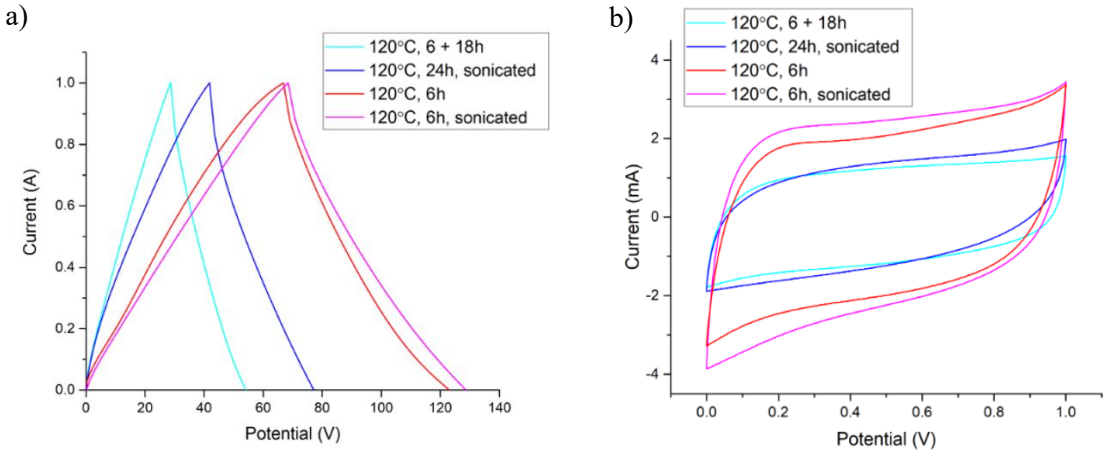

Figure 33. a) GCD plots of 4 rGO samples comparing the effects of sonication and reduction time at 1 A/g in 1 M H_2SO_4 b) CV plots of 4 rGO samples comparing the effects of sonication and reduction time using a scan rate of 50 mV/s in 1 M H_2SO_4.

Overall, from the hydrothermally reduced rGO electrodes, prepared from samples H2, H3 6h, H3 24h, H4, H5 6h, H7, H8 and H9, the GCD and CV measurements of all electrodes are presented below in figure 34 and capacitances were calculated from the GCD.

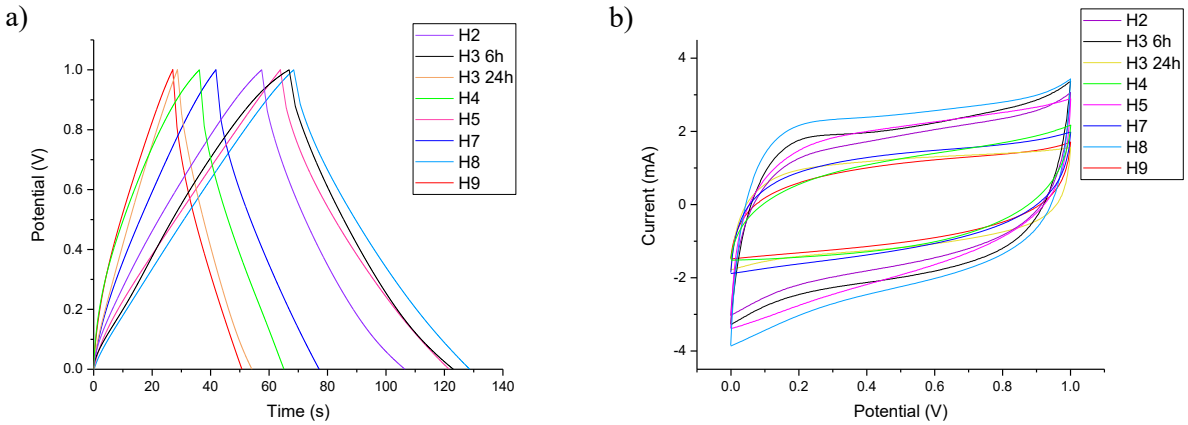

Figure 34.a) GCD plots of all rGO electrodes prepared from the hydrothermally reduced samples at 1 A/g in 1 M H_2SO_4 b) CV plots of all rGO electrodes prepared from the hydrothermally reduced samples using a scan rate of 50 mV/s in 1 M H_2SO_4.

Using the hydrothermal method, the highest capacitance is achieved with sample H8-rGO at 116.1 F/g. The higher capacitance most likely results from using a higher concentration of GO during reduction, sonication before reduction as well as 6 h uninterrupted reduction process. Based on the shape of the CV ad GCD graphs, the rGO seems to mainly have EDLC type

capacitance. All capacitances are listed in table 9 below. Samples prepared using the different methods will be compared to H8-rGO to compare the efficiency of the reduction methods.

Table 9. Specific and areal capacitances of the hydrothermally reduced rGO samples calculated from the GCD measurements.

Sample	C_s (F/g)	C_a (mF/cm^2)
H2	94.3	109
H3 6h	108.3	123
H3 24h	48.2	57
H4	54.6	67
H5 6h	111.5	128
H7	67.2	81
H8	116.1	131
H9	44.4	55

Chemical reduction

Studying the effect of reducing agent when preparing the rGO samples C1 and C2, a higher amount of $NaBH_4$ led to a slightly higher capacitance, both of which are also higher than H8. The sonochemical reduction used for C3 however shows notably lower capacitance. The GCD and CV measurements are shown in figure 35, and the calculated capacitances are presented in table 10 below.

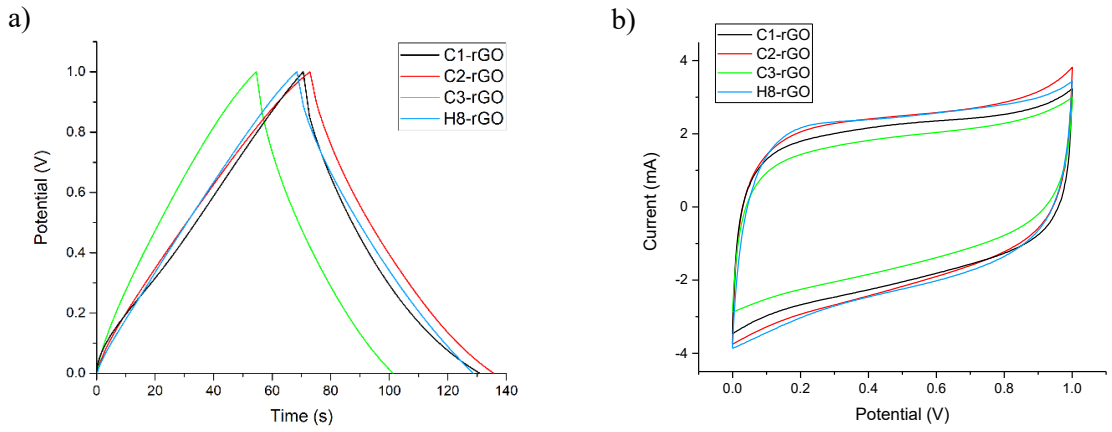

Figure 35. a) GCD plots of different chemically reduced rGO samples compared to the H8-rGO at 1 A/g in 1 M H_2SO_4 b) CV plots of different chemically reduced rGO samples compared to H8-rGO using scan rate 50 mV/s in 1 M H_2SO_4.

Table 10. Specific and areal capacitances of the chemically reduced rGO samples calculated from the GCD plots.

Sample	C_s (F/g)	C_a (mF/cm^2)
C1	116.5	137
C2	121.2	135
C3	89.9	103

Microwave reduction

From the microwave reduced rGO samples, electrodes were made from the reducedM4 and M5. The GCD and CV are presented in figure 36. Unfortunately, electrodes were not able to be made from M6 with the method we used as the rGO, as it would clump up and flake off from the electrode surface. The capacitances of the microwave reduced samples are much lower than H8; 64.5 F/g for M4 and 65.8 F/g for M5.

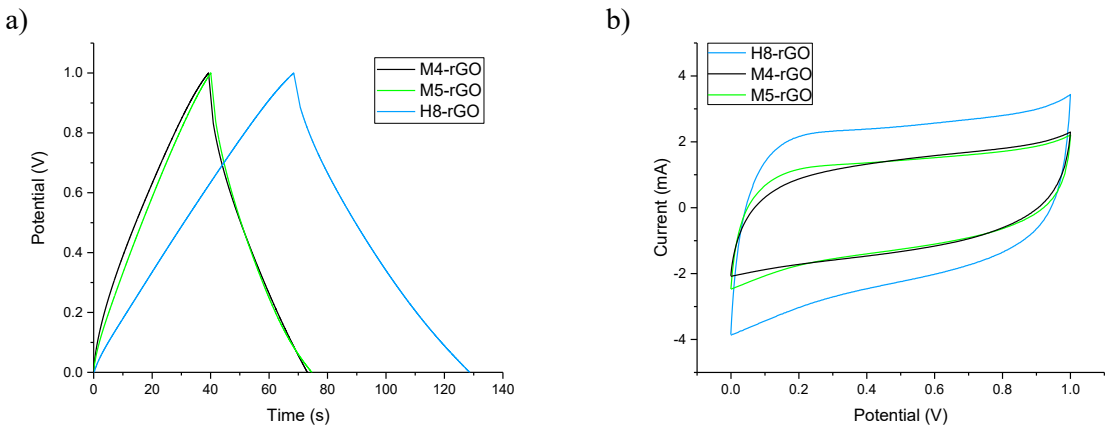

Figure 36.a) GCD of the microwave reduced rGO samples compared to H8-rGO at 1 A/g in 1 M H_2SO_4 b) CV plots of the microwave reduced samples compared to the H8-rGO at scan rate 50 mV/s in 1 M H_2SO_4.

Comparing the performances of all the different reducing methods based on their rGO's specific capacitance, microwave reduction performed significantly worse while chemical and hydrothermal methods were able to reach similar values. A comparison graph is presented in figure 37.

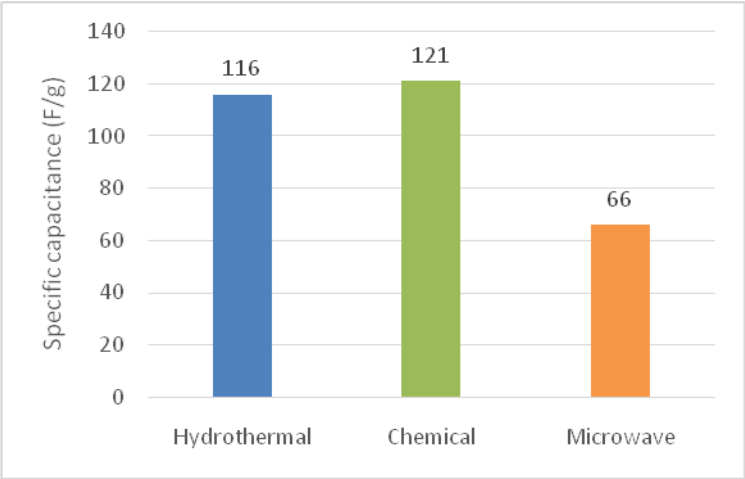

Figure 37. A vertical bar chart comparing the different reduction methods based on specific capacitance calculated from the GCDs.

Composite

GCD and CV measurements were done for all 3 composites, presented in figure 38 below. Comparing the CV and GCD of the different rGO-CNF composites to the H8-rGO used in the composite, the capacitance has lowered. Out of the composites, rGO-CNF-1 (AA, low charge CNF) has the lowest capacitance, with rGO-CNF-2 (AA, high charge CNF) and rGO-CNF-3 (Aalto Jaana's CNF) having a higher capacitance.

Differences between the CNF-2, CNF-3are small, but the TEMPO oxidized high charge cellulose performs slightly better, with a capacitance of 80.3 F/g. However, the difference is minuscule at 0.4 F/g which can also be caused from measurement error or from the electrode crafting process, or from the slight difference in structure noted in the XRD measurements. Areal and specific capacitances for each composite is presented in table 11.

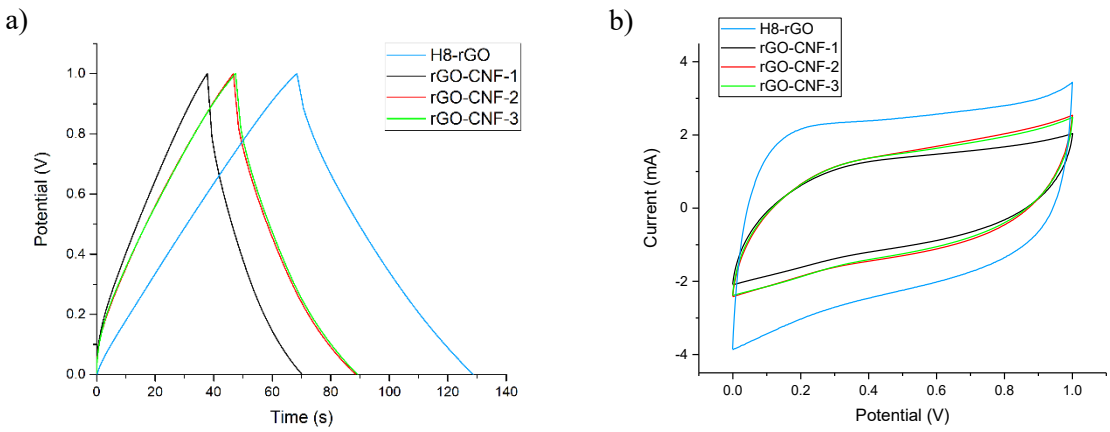

Figure 38. a) GCD measurements of the different composites and H8-rGOin 1 M H_2SO_4 at 1 A/g b) CV plots of the different composites and H8-rGO in 1 M H_2SO_4 at scan rate 50 mV/s.

Table 11. Specific and areal capacitances calculated from the composites' GCD measurements.

Composite	**C_p (F/g)**	**C_a (mF/cm^2)**
rGO-CNF-1	63.3	80
rGO-CNF-2	80.3	98
rGO-CNF-3	79.9	98

The performance of the pure rGO (H8) and the highest capacitive composite rGO-CNF-2 electrodes were also studied at different current densities ranging from 0.25 to 5 A/g presented in figure 39.

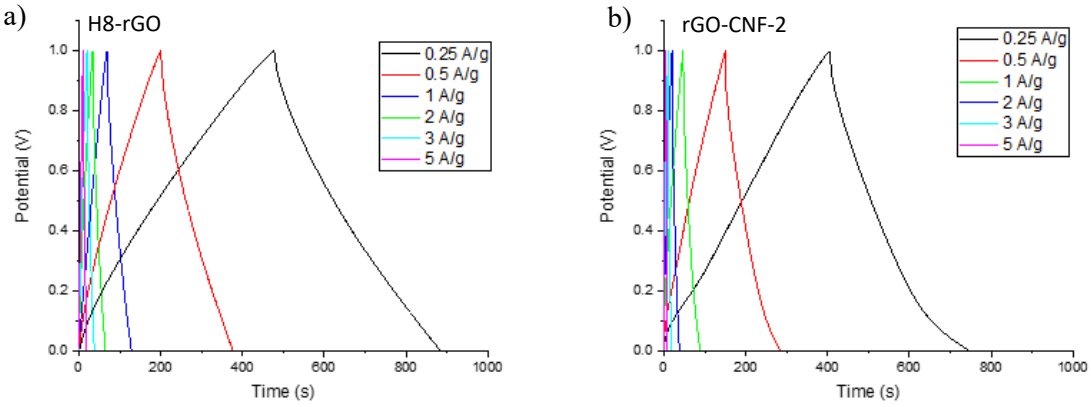

Figure. 39. a) GCD plots of H8-rGO in 1M H_2SO_4 electrolyte at different current densities b) GCD plots of rGO-CNF-2in 1 M H_2SO_4 electrolyte at different current densities.

The specific capacitances calculated from the GCD are presented together with the used current densities in figure 40. This further supports the claim that the pure rGO performs better compared to the composite. The capacitances also get higher when a lower current density is used, as the specific capacitances are highest at 0.25 A/g, with H8-rGO at 199.2 F/g and rGO-CNF-2 at 167.7 F/g, respectively. At a lower current density, the electrolyte ions have more time for the diffusion into the electrode materials pores resulting in a higher capacitance.

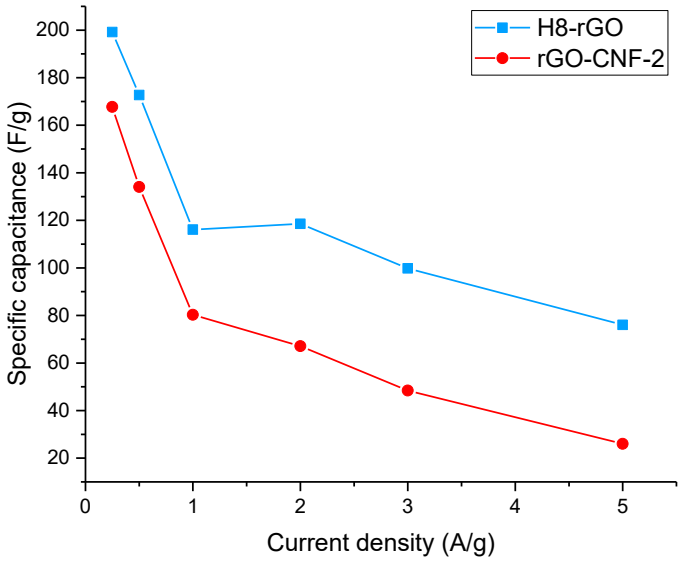

Figure 40. The specific capacitances of H8-rGO and rGO-CNF-2 at different current densities in 1 M H_2SO_4 electrolyte.

4 Conclusions

GO was successfully reduced using the hydrothermal method, with the minimum requirement for reduction being 3h at 120°C to produce rGO. The highest capacitance for rGO reaching 116 F/g at a current density of 1 A/g, was achieved for the sample reduced for 6h in 120°C using the hydrothermal method. This sample benefited from a higher concentration (2.5 mg/mL) along with a lower pH during reduction, and sonication before reduction as well as 6h reduction without breaks. A longer reduction time doesn't result in better capacitance, with the 24h reduced samples showing much lower capacitance, possibly due to agglomeration and the breaking down of the carbon network. Sonication is beneficial for the high capacitance of rGO materials, as well as slightly acidic/neutral pH rather than a basic pH. Studying the effects of concentration, higher pressure, sonication time and more acidic pH could be beneficial for our future studies.

The capacitance for rGO obtained using the hydrothermal method was slightly lower than what could be attained using chemical reduction with $NaBH_4$, but required more washing to remove the residual reducing agent and to reach a neutral pH. The highest capacitance gained using chemical reduction was 121 F/g at a current density of 1 A/g. Microwave reduction led to a low capacitance at 65 F/g, and reduction could not be done in a short time frame requiring at least 1h at the maximum 300 W of the reactor. All successfully reduced samples seem to show EDLC behavior under electrochemical conditions.

Composites were prepared using the hydrothermally reduced rGO sample with the highest capacitance, later combined with the CNF via a simple sonication process. Three different celluloses were used, but minimal differences could be seen both in structure and electrochemical measurements. rGO-CNF-2 and rGO-CNF-3 both had capacitances lower than the original rGO at approximately 80 F/g at a current density of 1 A/g. With a lower current density of 0.25 A/g the capacitance of the rGO was high at 199 F/g, and the composites (rGO-CNFs) were at 168 F/g, due to the electrolyte ions having more time to diffuse into the pores of the electrode material. Possible ways of enhancing the capacitance of the composite are incorporating the CNFs before reduction, or longer sonication when combining the rGO and CNF.

Self-standing films were also successfully formed using suction filtration. While a pure rGO film was unable to be removed from the supporting membrane, the composites were easily removed and were flexible, proving the CNF enhancing the mechanical strength.

References

1. Geim AK, Novoselov KS. The rise of graphene. *Nat Mater*. 2007;6(3):183-191. doi:10.1038/nmat1849
2. Pei S, Cheng H-M. The reduction of graphene oxide. *Carbon N Y*. 2012;50(9):3210-3228. doi:https://doi.org/10.1016/j.carbon.2011.11.010
3. Lee DW, De Los Santos V. L, Seo JW, et al. The Structure of Graphite Oxide: Investigation of Its Surface Chemical Groups. *J Phys Chem B*. 2010;114(17):5723-5728. doi:10.1021/jp1002275
4. Luo D, Zhang G, Liu J, Sun X. Evaluation Criteria for Reduced Graphene Oxide. *J Phys Chem C*. 2011;115(23):11327-11335. doi:10.1021/jp110001y
5. De Silva KKH, Huang H-H, Joshi RK, Yoshimura M. Chemical reduction of graphene oxide using green reductants. *Carbon N Y*. 2017;119:190-199. doi:https://doi.org/10.1016/j.carbon.2017.04.025
6. Huang H-H, De Silva KKH, Kumara GRA, Yoshimura M. Structural Evolution of Hydrothermally Derived Reduced Graphene Oxide. *Sci Rep*. 2018;8(1):6849. doi:10.1038/s41598-018-25194-1
7. Kramar A, González-Benito FJ. Cellulose-Based Nanofibers Processing Techniques and Methods Based on Bottom-Up Approach—A Review. *Polymers (Basel)*. 2022;14(2). doi:10.3390/polym14020286
8. Chen W, Yu H, Lee S-Y, Wei T, Li J, Fan Z. Nanocellulose: a promising nanomaterial for advanced electrochemical energy storage. *Chem Soc Rev*. 2018;47(8):2837-2872. doi:10.1039/C7CS00790F
9. Kötz R, Carlen M. Principles and applications of electrochemical capacitors. *Electrochim Acta*. 2000;45(15):2483-2498. doi:https://doi.org/10.1016/S0013-4686(00)00354-6
10. Bhat SA, Kumar V, Kumar S, Atabani AE, Anjum Badruddin I, Chae K-J. Supercapacitors production from waste: A new window for sustainable energy and waste management. *Fuel*. 2023;337:127125. doi:https://doi.org/10.1016/j.fuel.2022.127125
11. Wang Y, Song Y, Xia Y. Electrochemical capacitors: mechanism, materials, systems, characterization and applications. *Chem Soc Rev*. 2016;45(21):5925-5950. doi:10.1039/C5CS00580A
12. Gao K, Shao Z, Wu X, et al. Cellulose nanofibers/reduced graphene oxide flexible transparent conductive paper. *Carbohydr Polym*. 2013;97(1):243-251. doi:https://doi.org/10.1016/j.carbpol.2013.03.067
13. Gui Z, Zhu H, Gillette E, et al. Natural Cellulose Fiber as Substrate for Supercapacitor. *ACS Nano*. 2013;7(7):6037-6046. doi:10.1021/nn401818t
14. Park S, Ruoff RS. Chemical methods for the production of graphenes. *Nat Nanotechnol*.

2009;4(4):217-224. doi:10.1038/nnano.2009.58

15. Brodie BC. On the Atomic Weight of Graphite. *Philos Trans R Soc London*. 1859;149:249-259.
16. Staudenmaier L. Verfahren zur Darstellung der Graphitsäure. *Berichte der Dtsch Chem Gesellschaft*. 1898;31(2):1481-1487. doi:https://doi.org/10.1002/cber.18980310237
17. Hofmann U, König E. Untersuchungen über Graphitoxyd. *Zeitschrift für Anorg und Allg Chemie*. 1937;234(4):311-336. doi:https://doi.org/10.1002/zaac.19372340405
18. Hummers WSJ, Offeman RE. Preparation of Graphitic Oxide. *J Am Chem Soc*. 1958;80(6):1339. doi:10.1021/ja01539a017
19. Marcano DC, Kosynkin D V, Berlin JM, et al. Improved Synthesis of Graphene Oxide. *ACS Nano*. 2010;4(8):4806-4814. doi:10.1021/nn1006368
20. He H, Klinowski J, Forster M, Lerf A. A new structural model for graphite oxide. *Chem Phys Lett*. 1998;287(1):53-56. doi:https://doi.org/10.1016/S0009-2614(98)00144-4
21. Lerf A, He H, Forster M, Klinowski J. Structure of Graphite Oxide Revisited. *J Phys Chem B*. 1998;102(23):4477-4482. doi:10.1021/jp9731821
22. Chua CK, Pumera M. Chemical reduction of graphene oxide: a synthetic chemistry viewpoint. *Chem Soc Rev*. 2014;43(1):291-312. doi:10.1039/C3CS60303B
23. Buchsteiner A, Lerf A, Pieper J. Water Dynamics in Graphite Oxide Investigated with Neutron Scattering. *J Phys Chem B*. 2006;110(45):22328-22338. doi:10.1021/jp0641132
24. Jiříčková A, Jankovský O, Sofer Z, Sedmidubský D. Synthesis and Applications of Graphene Oxide. *Materials (Basel)*. 2022;15(3). doi:10.3390/ma15030920
25. Johra FT, Jung W-G. Hydrothermally reduced graphene oxide as a supercapacitor. *Appl Surf Sci*. 2015;357:1911-1914. doi:https://doi.org/10.1016/j.apsusc.2015.09.128
26. Chen J, Wang Y, Cao J, et al. Facile Co-Electrodeposition Method for High-Performance Supercapacitor Based on Reduced Graphene Oxide/Polypyrrole Composite Film. *ACS Appl Mater Interfaces*. 2017;9(23):19831-19842. doi:10.1021/acsami.7b03786
27. Tarcan R, Todor-Boer O, Petrovai I, Leordean C, Astilean S, Botiz I. Reduced graphene oxide today. *J Mater Chem C*. 2020;8(4):1198-1224. doi:10.1039/C9TC04916A
28. Syed N, Sharma N, Kumar L. Synthesis of Graphene Oxide (GO) by Modified Hummers Method and Its Thermal Reduction to Obtain Reduced Graphene Oxide (rGO) * Open Access. *Graphene*. 2017;6:1-18. doi:10.4236/graphene.2017.61001
29. Yang S, Lohe MR, Müllen K, Feng X. New-Generation Graphene from Electrochemical Approaches: Production and Applications. *Adv Mater*. 2016;28(29):6213-6221. doi:https://doi.org/10.1002/adma.201505326
30. Gengler RYN, Badali DS, Zhang D, et al. Revealing the ultrafast process behind the photoreduction of graphene oxide. *Nat Commun*. 2013;4(1):2560. doi:10.1038/ncomms3560
31. Jakhar R, Yap JE, Joshi R. Microwave reduction of graphene oxide. *Carbon N Y*.

2020;170:277-293. doi:https://doi.org/10.1016/j.carbon.2020.08.034

32. Kurtishaj Hamzaj A, Donà E, M Santhosh N, Shvalya V, Košiček M, Cvelbar U. Plasma-Modification of graphene oxide for advanced ammonia sensing. *Appl Surf Sci*. 2024;660:160006. doi:https://doi.org/10.1016/j.apsusc.2024.160006
33. Lavin-Lopez MP, Paton-Carrero A, Sanchez-Silva L, Valverde JL, Romero A. Influence of the reduction strategy in the synthesis of reduced graphene oxide. *Adv Powder Technol*. 2017;28(12):3195-3203. doi:https://doi.org/10.1016/j.apt.2017.09.032
34. Feng J, Ye Y, Xiao M, Wu G, Ke Y. Synthetic routes of the reduced graphene oxide. *Chem Pap*. 2020;74(11):3767-3783. doi:10.1007/s11696-020-01196-0
35. Guo H-L, Wang X-F, Qian Q-Y, Wang F-B, Xia X-H. A Green Approach to the Synthesis of Graphene Nanosheets. *ACS Nano*. 2009;3(9):2653-2659. doi:10.1021/nn900227d
36. Mokhena TC, Mochane MJ, Mtibe A, et al. Recent advances on nanocellulose-graphene oxide composites: a review. *Cellulose*. 2024;31(12):7207-7249. doi:10.1007/s10570-024-06055-9
37. Ding JN, Liu YB, Yuan NY, Ding GQ, Fan Y, Yu CT. The influence of temperature, time and concentration on the dispersion of reduced graphene oxide prepared by hydrothermal reduction. *Diam Relat Mater*. 2012;21:11-15. doi:https://doi.org/10.1016/j.diamond.2011.08.004
38. Zhou Y, Bao Q, Tang LAL, Zhong Y, Loh KP. Hydrothermal Dehydration for the "Green" Reduction of Exfoliated Graphene Oxide to Graphene and Demonstration of Tunable Optical Limiting Properties. *Chem Mater*. 2009;21(13):2950-2956. doi:10.1021/cm9006603
39. Sasikala SP, Poulin P, Aymonier C. Advances in Subcritical Hydro-/Solvothermal Processing of Graphene Materials. *Adv Mater*. 2017;29(22):1605473. doi:https://doi.org/10.1002/adma.201605473
40. Li X, Zhang G, Bai X, et al. Highly conducting graphene sheets and Langmuir–Blodgett films. *Nat Nanotechnol*. 2008;3(9):538-542. doi:10.1038/nnano.2008.210
41. Chen H, Song Z, Zhao X, Li X, Lin H. Reduction of free-standing graphene oxide papers by a hydrothermal process at the solid/gas interface. *RSC Adv*. 2013;3(9):2971-2978. doi:10.1039/C2RA21576D
42. Mei X, Meng X, Wu F. Hydrothermal method for the production of reduced graphene oxide. *Phys E Low-dimensional Syst Nanostructures*. 2015;68:81-86. doi:https://doi.org/10.1016/j.physe.2014.12.011
43. Bosch-Navarro C, Coronado E, Martí-Gastaldo C, Sánchez-Royo JF, Gómez MG. Influence of the pH on the synthesis of reduced graphene oxide under hydrothermal conditions. *Nanoscale*. 2012;4(13):3977-3982. doi:10.1039/C2NR30605K
44. Bai Y, Rakhi RB, Chen W, Alshareef HN. Effect of pH-induced chemical modification of hydrothermally reduced graphene oxide on supercapacitor performance. *J Power Sources*. 2013;233:313-319. doi:https://doi.org/10.1016/j.jpowsour.2013.01.122
45. Stankovich S, Piner RD, Chen X, Wu N, Nguyen ST, Ruoff RS. Stable aqueous dispersions of

graphitic nanoplatelets via the reduction of exfoliated graphite oxide in the presence of poly(sodium 4-styrenesulfonate). *J Mater Chem*. 2006;16(2):155-158. doi:10.1039/B512799H

46. Zou Z, Zhou W, Zhang Y, Yu H, Hu C, Xiao W. High-performance flexible all-solid-state supercapacitor constructed by free-standing cellulose/reduced graphene oxide/silver nanoparticles composite film. *Chem Eng J*. 2019;357:45-55. doi:https://doi.org/10.1016/j.cej.2018.09.143
47. Si Y, Samulski ET. Synthesis of Water Soluble Graphene. *Nano Lett*. 2008;8(6):1679-1682. doi:10.1021/nl080604h
48. Jiang X, Wang J, Guo J, Liu M, Fang Y. Reduction in Graphene Oxide by Sodium Borohydride for Enhanced BR13 Dye and Cu2+ Adsorption. *Arab J Sci Eng*. Published online 2022. doi:10.1007/s13369-022-06708-6
49. Fernández-Merino MJ, Guardia L, Paredes JI, et al. Vitamin C Is an Ideal Substitute for Hydrazine in the Reduction of Graphene Oxide Suspensions. *J Phys Chem C*. 2010;114(14):6426-6432. doi:10.1021/jp100603h
50. Zhang J, Yang H, Shen G, Cheng P, Zhang J, Guo S. Reduction of graphene oxide vial-ascorbic acid. *Chem Commun*. 2010;46(7):1112-1114. doi:10.1039/B917705A
51. De Silva KKH, Huang H-H, Yoshimura M. Progress of reduction of graphene oxide by ascorbic acid. *Appl Surf Sci*. 2018;447:338-346. doi:https://doi.org/10.1016/j.apsusc.2018.03.243
52. Zhu C, Guo S, Fang Y, Dong S. Reducing Sugar: New Functional Molecules for the Green Synthesis of Graphene Nanosheets. *ACS Nano*. 2010;4(4):2429-2437. doi:10.1021/nn1002387
53. Alazmi A, Rasul S, Patole SP, Costa PMFJ. Comparative study of synthesis and reduction methods for graphene oxide. *Polyhedron*. 2016;116:153-161. doi:https://doi.org/10.1016/j.poly.2016.04.044
54. Guex LG, Sacchi B, Peuvot KF, et al. Experimental review: chemical reduction of graphene oxide (GO) to reduced graphene oxide (rGO) by aqueous chemistry. *Nanoscale*. 2017;9(27):9562-9571. doi:10.1039/C7NR02943H
55. Ramachandran R, Saranya M, Velmurugan V, Raghupathy BPC, Jeong SK, Grace AN. Effect of reducing agent on graphene synthesis and its influence on charge storage towards supercapacitor applications. *Appl Energy*. 2015;153:22-31. doi:https://doi.org/10.1016/j.apenergy.2015.02.091
56. Zhu Y, Murali S, Stoller MD, Velamakanni A, Piner RD, Ruoff RS. Microwave assisted exfoliation and reduction of graphite oxide for ultracapacitors. *Carbon N Y*. 2010;48(7):2118-2122. doi:https://doi.org/10.1016/j.carbon.2010.02.001
57. Tien H, Van Hoang L, Cuong T, et al. Fast and Simple Reduction of Graphene Oxide in Various Organic Solvents Using Microwave Irradiation. *J Nanosci Nanotechnol*. 2012;12:5658-5662. doi:10.1166/jnn.2012.6340

58. Xiang X, Zhu Y, Yin M, Xia S, Guo C. Study of microwave reduction of graphene oxide suspension: structure and functional groups. *J Mater Sci*. 2022;57(5):3280-3294. doi:10.1007/s10853-021-06748-7
59. Murugan AV, Muraliganth T, Manthiram A. Rapid, Facile Microwave-Solvothermal Synthesis of Graphene Nanosheets and Their Polyaniline Nanocomposites for Energy Strorage. *Chem Mater*. 2009;21(21):5004-5006. doi:10.1021/cm902413c
60. Tien H, Van Hoang L, Hoa L, et al. The Rapid and Enhanced Reduction of Graphene Oxide by Microwave Assisted Acid Catalyzed Reaction. *J Nanosci Nanotechnol*. 2013;13:7104-7107. doi:10.1166/jnn.2013.7867
61. Bezerra Sandes Martins AL, Menezes Lima A, Rodrigues de Araújo J, Vieira Marques M de F, Anacleto Pinheiro W. Characterization of reduced graphene oxide by a hybrid ascorbic acid/microwave process in methyl-pyrrolidone dispersion. *MRS Commun*. 2022;12(5):924-929. doi:10.1557/s43579-022-00275-5
62. Chen W, Yan L, Bangal PR. Preparation of graphene by the rapid and mild thermal reduction of graphene oxide induced by microwaves. *Carbon N Y*. 2010;48(4):1146-1152. doi:https://doi.org/10.1016/j.carbon.2009.11.037
63. Kafy A, Kim HC, Zhai L, et al. Cellulose long fibers fabricated from cellulose nanofibers and its strong and tough characteristics. *Sci Rep*. 2017;7(1):17683. doi:10.1038/s41598-017-17713-3
64. Collard F-X, Blin J. A review on pyrolysis of biomass constituents: Mechanisms and composition of the products obtained from the conversion of cellulose, hemicelluloses and lignin. *Renew Sustain Energy Rev*. 2014;38:594-608. doi:https://doi.org/10.1016/j.rser.2014.06.013
65. Borsoi C, Zimmernnam MVG, Zattera AJ, Santana RMC, Ferreira CA. Thermal degradation behavior of cellulose nanofibers and nanowhiskers. *J Therm Anal Calorim*. 2016;126(3):1867-1878. doi:10.1007/s10973-016-5653-x
66. Isogai A, Saito T, Fukuzumi H. TEMPO-oxidized cellulose nanofibers. *Nanoscale*. 2011;3(1):71-85. doi:10.1039/C0NR00583E
67. Saito T, Kimura S, Nishiyama Y, Isogai A. Cellulose Nanofibers Prepared by TEMPO-Mediated Oxidation of Native Cellulose. *Biomacromolecules*. 2007;8(8):2485-2491. doi:10.1021/bm0703970
68. Siró I, Plackett D. Microfibrillated cellulose and new nanocomposite materials: a review. *Cellulose*. 2010;17(3):459-494. doi:10.1007/s10570-010-9405-y
69. Tingaut P, Zimmermann T, Sèbe G. Cellulose nanocrystals and microfibrillated cellulose as building blocks for the design of hierarchical functional materials. *J Mater Chem*. 2012;22(38):20105-20111. doi:10.1039/C2JM32956E
70. Zhang LL, Zhao XS. Carbon-based materials as supercapacitor electrodes. *Chem Soc Rev*.

2009;38(9):2520-2531. doi:10.1039/B813846J

71. Islam MR, Afroj S, Novoselov KS, Karim N. Smart Electronic Textile-Based Wearable Supercapacitors. *Adv Sci*. 2022;9(31):2203856. doi:https://doi.org/10.1002/advs.202203856
72. Zhong C, Deng Y, Hu W, Qiao J, Zhang L, Zhang J. A review of electrolyte materials and compositions for electrochemical supercapacitors. *Chem Soc Rev*. 2015;44(21):7484-7539. doi:10.1039/C5CS00303B
73. Shivakumara S, Kishore B, Penki TR, Munichandraiah N. Symmetric supercapacitor based on partially exfoliated and reduced graphite oxide in neutral aqueous electrolyte. *Solid State Commun*. 2014;199:26-32. doi:https://doi.org/10.1016/j.ssc.2014.08.014
74. Ogoshi T, Yoshikoshi K, Sueto R, Nishihara H, Yamagishi T. Porous Carbon Fibers Containing Pores with Sizes Controlled at the Ångstrom Level by the Cavity Size of Pillar[6]arene. *Angew Chemie Int Ed*. 2015;54(22):6466-6469. doi:https://doi.org/10.1002/anie.201501854
75. Lin Z, Liu Y, Yao Y, et al. Superior Capacitance of Functionalized Graphene. *J Phys Chem C*. 2011;115(14):7120-7125. doi:10.1021/jp2007073
76. Frackowiak E, Béguin F. Carbon materials for the electrochemical storage of energy in capacitors. *Carbon N Y*. 2001;39(6):937-950. doi:https://doi.org/10.1016/S0008-6223(00)00183-4
77. Pholauyphon W, Charoen-amornkitt P, Suzuki T, Tsushima S. Guidelines for supercapacitor electrochemical analysis: A comprehensive review of methodologies for finding charge storage mechanisms. *J Energy Storage*. 2024;98:112833. doi:https://doi.org/10.1016/j.est.2024.112833
78. Xing J, Tao P, Wu Z, Xing C, Liao X, Nie S. Nanocellulose-graphene composites: A promising nanomaterial for flexible supercapacitors. *Carbohydr Polym*. 2019;207:447-459. doi:https://doi.org/10.1016/j.carbpol.2018.12.010
79. Bacakova L, Pajorova J, Tomkova M, et al. Applications of Nanocellulose/Nanocarbon Composites: Focus on Biotechnology and Medicine. *Nanomaterials*. 2020;10(2). doi:10.3390/nano10020196
80. Patel JP, Parsania PH. 3 - Characterization, testing, and reinforcing materials of biodegradable composites. In: Shimpi NGBT-B and BPC, ed. *Woodhead Publishing Series in Composites Science and Engineering*. Woodhead Publishing; 2018:55-79. doi:https://doi.org/10.1016/B978-0-08-100970-3.00003-1
81. He W, Wu B, Lu M, Li Z, Qiang H. Fabrication and Performance of Self-Supported Flexible Cellulose Nanofibrils/Reduced Graphene Oxide Supercapacitor Electrode Materials. *Molecules*. 2020;25(12):2793. doi:10.3390/molecules25122793
82. Waremra R, Betaubun P. Analysis of Electrical Properties Using the four point Probe Method. *E3S Web Conf*. 2018;73:13019. doi:10.1051/e3sconf/20187313019

Supplementary information

Table S1. Details of the electrode preparation

Sample	Final V (mL)	Final c(rGO) (mg/mL)	Method	m(rGO) (mg)	V(rGO) (mL)	V(Nafion) (µL)
H2	44	1.45	coating	1	0.685	5
			ink	1	0.685	5
H3	57	0.42	ink	1	2.375	5
H3-24h	45	1.08	ink	1	0.93	5
H4-18h	36	0.98	ink	1	0.78	10
H5-6h	43	1.02	ink	1	0.96	5
H7	47	1.04	ink	1	0.964	5
H8	20	1.79	ink	1	0.56	5
H9-3h	10	1	ink	1	1	5
C1	22.5	2.22	coating	1	0.45	10
C2	15.5	3.23	coating	1	1.35	10
C3	2	5	ink	1	0.31	5
M1	2	1.25	ink	1	0.8	5
M2	1.1	1.25	ink	1	0.8	5
rGO-CNF-1	10	1	ink	1	1	5
rGO-CNF-2	20	0.5	ink	1	2	5
rGO-CNF-3	23	0.43	ink	1	2.3	5

Table S2. The used reaction temperature, applied pressure (N_2) and final pressure during the hydrothermal reduction

Temperature (°C)	Starting pressure (bar)	Final pressure (bar)
80	7	7
120	7	9
150	7	10
180	0	9
180	7	13
220	7	22